Epigenetic memory is governed by an effector recruitment specificity toggle in Heterochromatin Protein 1

Amanda Ames[1], Melissa Seman[1], Ajay Larkin[1], Gulzhan Raiymbek[2], Ziyuan Chen[3], Alex Levashkevich[1], Bo Kim[4], Julie Suzanne Biteen[3,5], and Kaushik Ragunathan[1*]

[1] Department of Biology, Brandeis University, Waltham, MA 02453

[2] Department of Biological Chemistry, University of Michigan, Ann Arbor, MI 48109

[3] Department of Biophysics, University of Michigan, Ann Arbor, MI 48104

[4] Department of Biochemistry, Brandeis University, Waltham, MA 02453

[5] Department of Chemistry, University of Michigan, Ann Arbor, MI 48104

These authors contributed equally: Melissa Seman, Ajay Larkin

* Correspondence: kaushikr@brandeis.edu (K.R.)

ABSTRACT

HP1 proteins are essential for establishing and maintaining transcriptionally silent heterochromatin. They dimerize, forming a binding interface to recruit diverse chromatin-associated factors. HP1 proteins are specialized and rapidly evolve, but the extent of variation required to achieve functional specialization is unknown. To investigate how changes in amino acid sequence impacts epigenetic inheritance, we performed a targeted mutagenesis screen of the S. pombe HP1 homolog, Swi6. Substitutions within an auxiliary surface adjacent to the HP1 dimerization interface produced Swi6 variants with divergent maintenance properties. Remarkably, substitutions at a single amino acid position led to the persistent gain or loss of epigenetic inheritance. These substitutions increased Swi6 chromatin occupancy *in vivo* and altered Swi6-protein interactions that reprogram H3K9me maintenance. We show that relatively minor changes in Swi6 amino acid composition can lead to profound changes in epigenetic inheritance which provides a redundant mechanism to evolve novel effector specificity.

INTRODUCTION

Chromatin organization is critical for maintaining genome integrity and regulating gene expression[1]. Establishing distinct chromatin compartments consisting of active or repressed genes depends, in part, on the post-translational modifications of DNA packaging proteins called histones[2-4]. Inheriting chromatin states following DNA replication enables cells to maintain their unique identities[5,6]. Disrupting the epigenetic regulatory landscape leads to aneuploidy and genome instability, which are established hallmarks of cancer[7]. Over 50% of all sequenced cancers have at least a single mutation in core histones, histone-binding proteins, or nucleosome remodelers, underscoring the devastating impacts of epigenetic misregulation in cancer[8]. Therefore, advancing our knowledge of how epigenetic states are established and maintained is critical to illuminate normal cellular physiology and potentially develop novel, innovative therapeutic strategies.

Site-specific DNA or RNA binding proteins recruit histone modifiers to target unique locations in the genome to place repressive histone modifications as part of a process referred to as "*establishment*"[9]. These repressive modifications can then be propagated over multiple cell divisions in a DNA sequence-independent manner through a process known as "*maintenance"* or "*epigenetic inheritance*". The molecular basis for epigenetic inheritance is thought to involve the random but equal partitioning of modified H3-H4 parental histones between daughter DNA strands during each cycle of DNA replication[10-13]. In this model, modified histones are expected to serve as templates to restore pre-existing histone modification states on newly synthesized DNA[14]. Histone-modifying enzymes restore these states by engaging in a process called 'read-write' wherein pre-existing histone modifications can recruit enzymes to modify newly incorporated histones[15-19]. However, in addition to the enzyme having read-write properties, several non-histone proteins that bind to H3K9me have also been implicated in regulating epigenetic inheritance, in particular by inducing changes in chromatin conformation[20,21]. For example, *in vitro* reconstitution studies show that PRC1 (polycomb repressive complex 1), a

55 protein complex that belongs to the Polycomb group (PcG) and is involved in H3K27 (histone
56 H3 lysine 27) methylation (H3K27me) dependent silencing, remains continuously bound to old
57 and newly replicated DNA independent of H3K27me[22]. Furthermore, the ability of PRC1 to
58 undergo liquid-liquid phase separation and form condensates in conjunction with modified
59 histones can tune epigenetic memory[23]. In an analogous silencing pathway, proteins called
60 Heterochromatin Protein 1 (HP1) recognize and bind to histone H3 lysine 9 (H3K9) methylation
61 (H3K9me), remain bound to their cognate chromatin marks both before and after DNA
62 replication, suggesting that HP1 proteins might be part of the epigenetic imprint[24]. HP1 proteins
63 can also undergo phase separation, and their ability to oligomerize is crucial for maintaining
64 epigenetic memory[25,26]. Collectively, these results suggest that proteins that can drive changes
65 in chromatin organization contribute to the inheritance of modified chromatin states. However,
66 the mechanisms that coordinate the interplay between histone and non-histone proteins to
67 enable epigenetic inheritance remain poorly understood.
68 Reader domains that recognize and bind to specific histone modifications play important
69 roles in specifying the transcriptional context of an epigenetic state[27]. Canonical reader
70 domains, such as bromodomains, chromodomains, and Tudor domains, are part of protein
71 complexes that moderate gene expression and chromatin accessibility[28]. Intriguingly, some
72 reader domain paralogs bind to the same mark yet produce opposite transcriptional outcomes[29].
73 Many regulatory mechanisms contribute to this diversity, including multivalent interactions with
74 nucleosomes, RNA or DNA, autoinhibition driving protein conformational changes, and
75 cooperative binding to combinations of histone modifications[30-32]. Readers are enigmatic
76 because, despite being highly conserved, their ability to be co-opted by diverse effectors
77 enables them to fulfill functionally distinct roles in regulating gene expression[33]. Further, the
78 aforementioned processes thought to regulate epigenetic inheritance; such as “read-write”,
79 oligomerization, and phase separation; accomplish this by co-opting reader domain containing

proteins (such as HP1), These observations underscore the critical role that reader domains have in promoting epigenetic inheritance.

A pivotal reader domain-containing protein involved in heterochromatin formation is heterochromatin protein 1 (HP1)[34]. HP1 proteins have both a conserved chromodomain (CD), which binds specifically to H3K9me, and a chromoshadow domain (CSD) that promotes dimerization[35,36]. HP1 proteins can engage in higher-order interactions, leading to the formation of condensates that have liquid-like or gel-like properties *in vitro* and *in vivo*[37-40]. Although its physiological relevance remains an active area of investigation, one possibility is that the ability of HP1 proteins to form condensates leads to the assembly of distinct compartments that increase the local concentrations of silencing factors while selectively excluding transcriptional activators[26,41,42]. Upon dimerization, the CSD subunits also create a binding interface that facilitates protein interactions[43]. HP1 proteins typically bind to proteins containing variations of a consensus pentapeptide motif, with the defining feature in most cases being a central valine residue, such as the PxVxL motif in mouse CAF1 or the LxVxI motif present in the *Drosophila* HP2 protein[44,45]. Some HP1 variants demonstrate altered specificity for binding partners that contain degenerate equivalents of this motif. Notably, the *S. pombe* HP1 paralog Chp2 binds to a chromatin remodeler Mit1 through a CkIvV motif[46]. HP1 proteins recruit factors that both enhance and antagonize heterochromatin formation, many of which bind to the same shared CSD interface[47,48]. This raises an important question about how the recruitment of factors with opposing activities is coordinated, given that all these effectors presumably compete for the same CSD interface.

HP1 proteins are among the most rapidly evolving protein families[49,50]. An instance of this evolutionary dynamic is seen in Dipteran flies[50]. Phylogenomic studies reveal an unusually high number of HP1 gene duplications, leading to new opportunities for functional specialization of paralogs. These young HP1 genes show an elevated percent identity at amino acid positions involved in histone modification recognition and protein dimerization, indicating they are

106 functional HP1 paralogs that evolved through positive selection[50]. In contrast, across HP1
107 paralogs, and to a more considerable extent between HP1 orthologs, there is substantial
108 variation in amino acid residues at positions within the CD and CSD that are functionally
109 undefined[32,44]. Non-conserved sequences could contribute to functional diversity in HP1 proteins
110 by influencing some paralog-specific functions. In mouse HP1a, the N-terminal extension serves
111 as a site for hyperphosphorylation, which leads to higher chromatin binding and compaction[51].
112 The strength of CSD dimerization, which can be influenced by amino acid composition in the
113 CSD and C-terminal extension, can differ across HP1 proteins and is thought to tune their
114 affinity for various protein ligands[32,52,53]. However, we have limited knowledge of how much
115 sequence variation is required to alter the function of HP1 proteins and achieve specialization.
116 The fission yeast *Schizosacchromyces pombe* (*S. pombe*) represents an outstanding
117 model system to study heterochromatin[54]. Heterochromatin establishment and maintenance
118 involves H3K9 methylation and the enzymatic activity of an H3K9 methyltransferase in *S.*
119 *pombe* called Clr4, a Suv39h homolog[55]. *S. pombe* has two HP1 reader proteins, Chp2 and
120 Swi6, with extensive sequence similarity and shared structural similarities to HP1 proteins in
121 metazoans, including an H3K9me binding chromodomain (CD) and a dimerization domain
122 (CSD)[56-58]. Swi6 and Chp2 have distinct yet additive roles in transcriptional silencing at
123 pericentromeric repeats, telomeres, and the mating type locus[59]. The two HP1 proteins interact
124 with distinct sets of heterochromatin regulators and have vastly different expression levels (Swi6
125 is expressed 100-fold higher than Chp2)[60]. Swi6 interacts with many factors, including those
126 involved in RNAi-mediated heterochromatin formation, the histone deacetylase (Clr3), and a
127 putative H3K9 demethylase (Epe1)[47,61-66]. Chp2 recruits the Snf2/HDAC repressive effector
128 complex (SHREC) that includes Clr3 and the chromatin remodeler Mit1 to promote
129 transcriptional silencing[18,46,59,67]. Given the potential role of reader proteins, such as Swi6, in
130 epigenetic inheritance, we anticipate that their plasticity to evolve new protein-protein
131 interactions could serve as a potential mechanism to tune epigenetic memory.

132 In this work, we determine how sequence changes in Swi6 influence epigenetic
133 inheritance by performing a targeted PCR-based mutagenesis screen. By modifying the amino
134 acid composition in the Swi6-CSD through a targeted, PCR-based mutagenesis strategy, we
135 alter the durability of H3K9me-dependent epigenetic inheritance. Notably, we show substitutions
136 at a single residue (Thr 278) are sufficient to achieve complete functional divergence. While
137 some amino acid substitutions at this residue produce a gain of function maintenance
138 phenotype, other substitutions at the same site result in a persistent loss of function phenotype.
139 Furthermore, we demonstrate that a gain of function substitution leads to specific alterations in
140 protein-protein interactions that are known to regulate epigenetic inheritance; including a loss of
141 interaction with the putative H3K9 demethylase Epe1and a gain of interaction with the rixosome
142 complex, a central component of ribosome biogenesis which is required for heterochromatin
143 inheritance[21,68]. Additionally, these substitutions alter Swi6 chromatin occupancy *in vivo*. Our
144 study reveals that an HP1 protein, and possibly other reader proteins alike, can display
145 substantial plasticity wherein relatively minor variations in amino acid composition outside
146 primary structural interfaces can produce strikingly different functional outcomes.

147 **RESULTS**

148 **Novel Swi6 variants affect heterochromatin maintenance.**

149 To uncouple the effects of sequence-dependent heterochromatin establishment from
150 epigenetic inheritance, we used a system where a TetR-Clr4-I fusion protein binds to *10X-tetO*
151 DNA binding sequences placed upstream of an *ade6+* reporter gene. TetR-Clr4-I binding allows
152 for site-specific H3K9me deposition, leading to H3K9me establishment and *ade6+*
153 silencing[15,18,69]. Cells appear red on low adenine media when *ade6+* is silenced and white when
154 *ade6+* is expressed. The addition of tetracycline (+tet) triggers the release of TetR-Clr4-I, after
155 which we can measure epigenetic inheritance without continuous initiation (**Figure 1a**).
156 Consistent with previous work, deleting the eraser of H3K9me, Epe1 (*epe1Δ)*, is necessary to
157 maintain *ade6+* silencing, as indicated by the appearance of red and sectored colonies that

158 persist on +tetracycline-containing medium in contrast to white colonies in *epe1+* cells (**Figure**
159 **1b**, *epe1+* versus *epe1*Δ*,* +tet)[18].
160 To determine the role of Swi6 in epigenetic inheritance, we generated a site-directed
161 mutagenesis library using tiling primers containing degenerate NNN codons for each amino acid
162 position. Since it is the primary interaction site for heterochromatin-associated factors, we
163 focused our mutagenesis efforts on the Swi6-CSD, consisting of 65 amino acids. This PCR-
164 based *swi6-CSD* variant library was integrated into the *S. pombe* genome to replace the
165 endogenous *swi6+* sequence (**Supplementary Figure 1a**). To identify Swi6 gain-of-function
166 mutations that lead to enhanced maintenance, we transformed our *swi6*-CSD variant library in
167 an *epe1+* background where cells are normally white when plated on +tet medium. We
168 expected a gain-of-function Swi6 variant to produce red/sectored colonies on +tet medium.
169 Based on an initial hit in our screen (T278Y), we discovered that several Thr 278 substitutions
170 produced a gain-of-function maintenance phenotype, including phenylalanine (F), tyrosine (Y),
171 alanine (A), cysteine (C), and serine (S) (**Figure 1b**). This subset of residues are all conserved
172 or semi-conserved substitutions with uncharged side chains (A, C, F, S, Y). When Thr 278 was
173 replaced with amino acid substitutions containing charged side chains- we observed a gain of
174 maintenance in the case of glutamate (E) and arginine (R) substitutions, but unexpectedly, we
175 observed a loss of maintenance in the case of aspartate (D) and lysine (K) substitutions (**Figure**
176 **1c**). These phenotypic differences were not due to changes in Swi6 protein levels, given that the
177 expression of all Thr 278 variants is comparable to Swi6-WT protein (**Supplementary Figure**
178 **1b-c**).
179 We quantitatively measured transcriptional silencing of the reporter locus in *swi6* T278Y
180 (*swi6*-Y*)* and *swi6* T278K (*swi6*-K*)*. We performed quantitative real-time PCR (qRT-PCR) on the
181 gene upstream of *10XTetO-ade6*, *SPCC330.06c*. Consistent with the *ade6+* silencing
182 phenotype, *swi6*-Y*,* and *swi6*-K showed a similar decrease in RNA expression as observed in
183 *swi6*-WT (**Figure 1d**). After 24 hours of growth in +tet, we observed the maintenance of reduced

184 transcript levels in *swi6*-Y consistent with a gain of heterochromatin maintenance. Conversely,
185 *swi6*-K cells showed increased transcript levels consistent with no heterochromatin
186 maintenance (**Figure 1d**). We also measured H3K9me3 levels at *SPCC330.06c* using
187 chromatin immunoprecipitation followed by qPCR (ChIP-qPCR) before and after adding
188 tetracycline. As expected, we observed high H3K9me3 enrichment in the context of
189 establishment (-tet) in both *swi6*-Y and *swi6*-K. In contrast, H3K9me3 persisted during
190 maintenance (+tet) in the case of *swi6*-Y but not *swi6*-K (**Figure 1e**).
191 As mentioned previously, heterochromatin maintenance in our reporter system is
192 critically dependent on the absence of H3K9me eraser Epe1, with *epe1*Δ cells being the primary
193 genetic context in which we observed red or sectored colonies on +tet media. To determine if
194 the observed maintenance phenotypes in *swi6*-Y and *swi6*-K are dependent on Epe1, we
195 deleted Epe1 in both genetic backgrounds. We expected that *swi6*-Y gain-of-maintenance
196 would either be unaffected or further enhanced by *epe1*Δ, whereas *swi6*-K would acquire a
197 maintenance phenotype upon deleting *epe1*. Unexpectedly, maintenance was not restored in
198 *swi6*–K *epe1*Δ cells, as indicated by the continued appearance of white colonies in +tet medium
199 matching what we see in *swi6*-K *epe1+* cells. Although *epe1*Δ is sufficient to confer
200 heterochromatin maintenance in *swi6*-WT cells, it fails to produce a maintenance phenotype in
201 *swi6*-K expressing cells (**Figure 1f, Supplementary Figure 1d**). It is also noteworthy that *swi6*-
202 Y *epe1*Δ cells exhibited a slightly weaker epigenetic maintenance phenotype with fewer
203 sectored colonies than *swi6*-Y *epe1+* cells. Nevertheless, deleting *epe1*Δ in *swi6*-Y did not
204 completely disrupt maintenance since we still observed persistent transcriptional silencing
205 consistent with successful maintenance when cells were plated on +tet media (**Figure 1f,**
206 **Supplementary Figure 1d**). Based on these findings, we concluded that *swi6*-Y has a
207 persistent gain-of-function maintenance phenotype, whereas *swi6*-K, unlike *swi6*-WT, has a
208 persistent loss-of-function maintenance phenotype.

209 One possibility is that Swi6 phosphorylation is affected by Thr 278 substitutions. We
210 tested the effect of deleting Ckb1, a subunit of the casein kinase II complex (CK2) in *S. pombe*
211 that phosphorylates Swi6. Ckb1-mediated phosphorylation leads to the disruption of
212 heterochromatin silencing by inhibiting recruitment of the histone deacetylase Clr3 while
213 concomitantly upregulating Epe1 occupancy at sites of heterochromatin formation[70]. Upon
214 deleting the CK2 subunit, *ckb1* (*ckb1*Δ), *ade6+* silencing is lost in both *swi6*-WT and *epe1*Δ
215 cells. Surprisingly, heterochromatin silencing remains intact in *ckb1*Δ *swi6*-Y cells, suggesting
216 Swi6-Y gain-of-maintenance is not regulated by CK2 phosphorylation (**Figure 1g**).

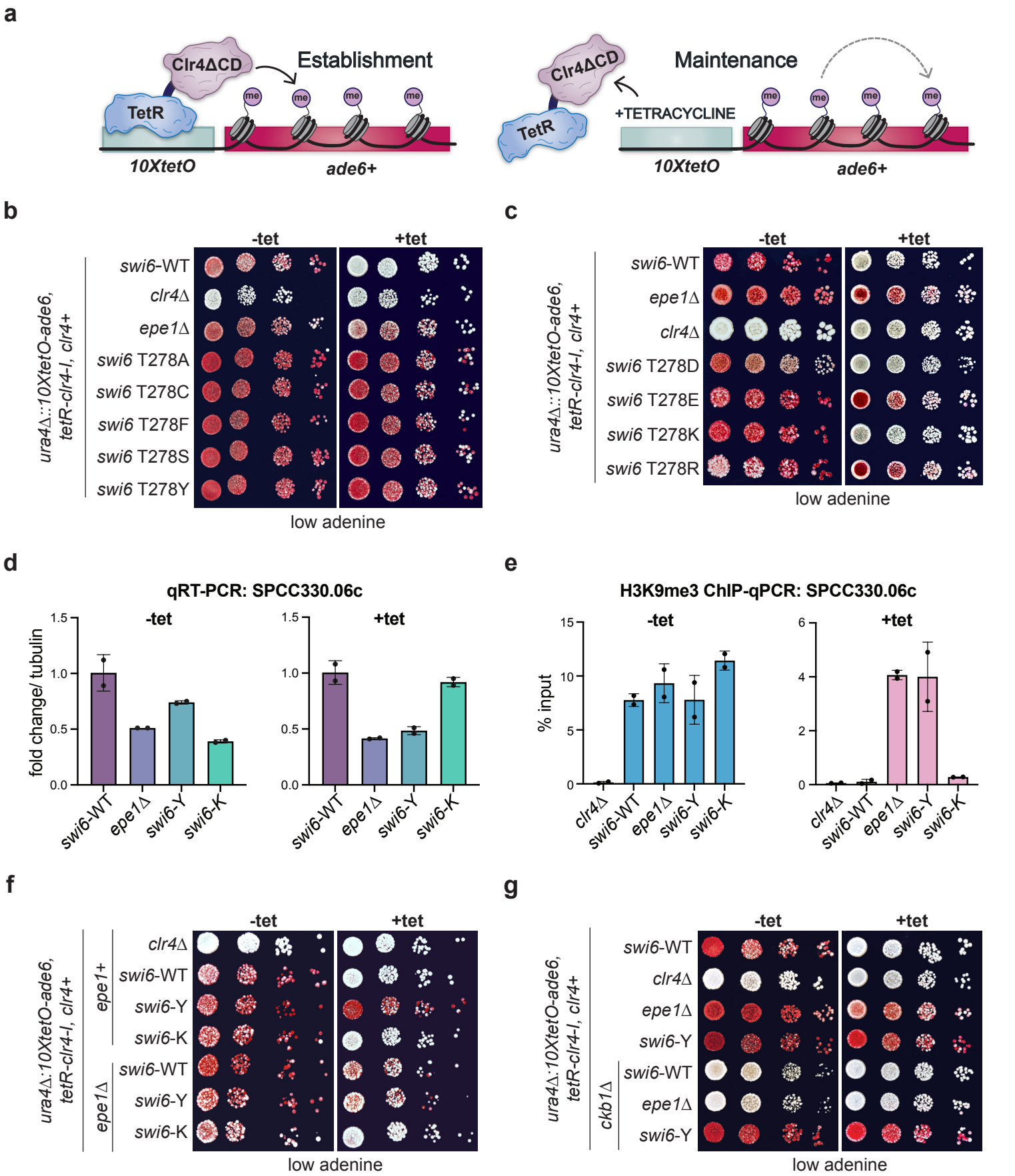

Figure 1. Novel Swi6 variants affect heterochromatin maintenance. (a) Schematic of TetR-Clr4-I recruitment to *10XtetO* binding sites upstream of an *ade6+* reporter gene, initiating heterochromatin establishment. Addition of tetracycline (+tet) releases TetR-Clr4-I, enabling measurements of heterochromatin maintenance uncoupled from sequence-specific establishment. **(b-c)** Silencing assay of *ura4Δ::10XtetO-ade6+* reporter in indicated genotypes in the absence (-tet) and presence (+tet) of tetracycline. Red cells indicate ade6+ silencing. Cells are plated as 10-fold serial dilutions. **(d)** qRT-PCR measuring RNA levels at SPCC330.06c in indicated genotypes before (-tet) and after (+tet) tetracycline addition. Error bars indicate SD (N = 2). **(e)** ChIP-qPCR measuring H3K9me3 at *SPCC330.06c* in indicated genotypes before (-tet) and after (+tet) tetracycline addition. Error bars indicate SD (N = 2). **(f-g)** Silencing assay of *ura4Δ::10XtetO-ade6+* reporter in indicated genotypes in the absence (-tet) and presence (+tet) of tetracycline. Red cells indicate *ade6+* silencing. Cells are plated at 10-fold serial dilutions.

217 **Maintenance in Swi6-Y depends on H3K9me.**

218 To determine how *swi6*-Y or *swi6*-K substitutions affect heterochromatin spreading and
219 its epigenetic inheritance, we performed chromatin immunoprecipitation followed by sequencing
220 (ChIP-seq) of H3K9me2 and H3K9me3. We observed large H3K9me domains consistent with
221 successful heterochromatin establishment proximal to the *10XtetO-ade6* reporter site across all
222 Swi6 variant backgrounds (**Figure 2a-b**). Upon +tet treatment, H3K9me2 and H3K9me3 levels
223 are maintained only in *swi6*-Y like what we observed in *epe1*Δ cells and completely lost in *swi6*-
224 K like what we typically observe in *swi6*-WT (**Figure 2a-b**). These results suggest that the gain
225 of maintenance phenotype we observed in *swi6*-Y is dependent on the inheritance of H3K9me.

226 To determine the extent to which both Swi6 variants affect constitutive heterochromatin,
227 we replaced the endogenous *swi6+* gene with *swi6*-Y and *swi6*-K in cells where an *ade6+*
228 reporter was inserted at the pericentromeric outer repeats (*otr1R(SphI)::ade6+)* (**Figure 2c**).
229 Unlike *swi6*-WT cells that appeared uniformly red, we observed a small proportion of white,
230 *ade6+* expressing colonies in *swi6*-Y and *swi6*-K, suggesting a minor defect in pericentromeric
231 reporter gene silencing. These minor silencing defects were also mirrored in our qRT-PCR
232 analysis of pericentromeric (*dg* and *dh*) and telomeric (*tlh1*) transcripts (**Figure 2d**).
233 Nevertheless, enrichment for H3K9me2 and H3K9me3 at pericentromeres were comparable in
234 *swi6*-Y and *swi6*-K expressing cells (**Figure 2e, Supplementary Figure 2a-d**) while slightly
235 decreased at telomeres in *swi6*-Y and *swi6*-K compared to *swi6*-WT cells. H3K9me2 and
236 H3K9me3 levels at the rDNA locus were elevated in s*wi6*-Y but not in *swi6*-K, compared to
237 *swi6*-WT (**Supplementary Figure 2a-d**). We also observed elevated H3K9me2 and H3K9me3
238 enrichment at facultative heterochromatin islands such as meiotic genes (*mei4* and *ssm4*) in
239 *swi6*-K cells compared to *swi6*-WT (**Supplementary Figure 2e-f**).

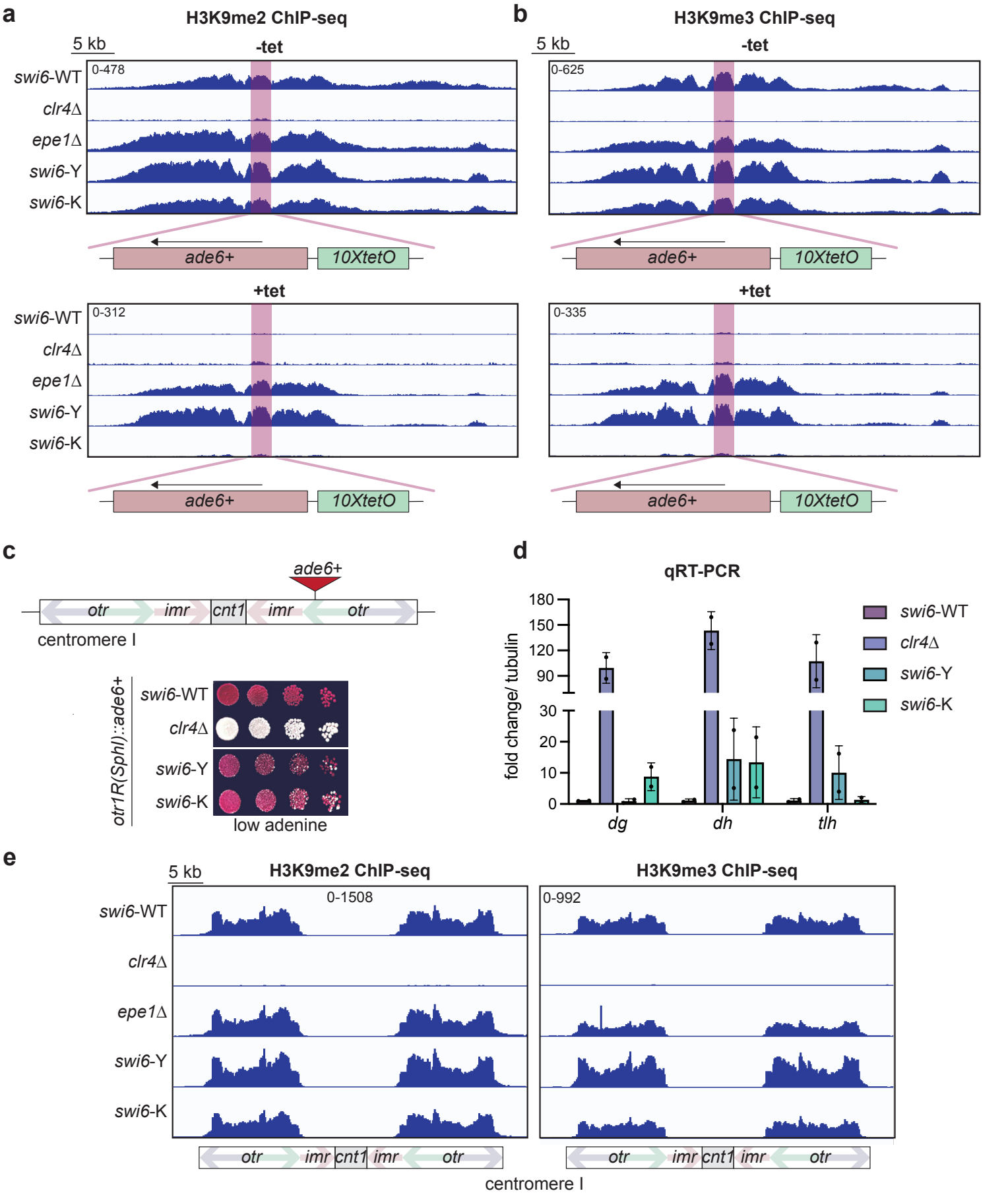

Figure 2. Maintenance in Swi6-Y depends on H3K9me. (**a-b**) ChIP-seq of H3K9me2 (**a**) and H3K9me3 (**b**) surrounding the *ura4Δ::10XtetO-ade6+* reporter in indicated genotypes and tetracycline treatment. The *ura4Δ::10XtetO-ade6+* reporter is highlighted in red. Each ChIP-seq track corresponds to a 40kb region. Enrichment in all samples is shown as normalized reads per kilobase million (RPKM). (**c**) Top- Schematic detailing the *otr1R::ade6+* reporter, where *ade6+* is inserted within the outer pericentromeric repeats. Bottom- Silencing assay of *otr1R::(SphI)ade6+* reporter in indicated genotypes. (**d**) qRT-PCR measuring RNA levels at *dg*, *dh*, and *tlh* in indicated genotypes and tetracycline treatment. Error bars indicate SD (N = 2). (**e**) ChIP-seq of H3K9me2 and H3K9me3 at the centromere on chromosome 1 in indicated genotypes. Each ChIP-seq track corresponds to a 45kb region with features within the centromere indicated in the schematic below. Enrichment in all samples is shown as normalized reads per kilobase million (RPKM).

240 **Swi6-Y and Swi6-K variants disrupt a direct interaction with Epe1**

241 As previously noted, deleting *epe1*Δ did not affect the maintenance phenotypes
242 associated with Swi6-Y (gain-of-maintenance) or Swi6-K (loss-of-maintenance). We reasoned
243 that our Thr 278 substitutions might disrupt a direct binding interaction between Epe1 and Swi6
244 while leaving other binding interactions required for heterochromatin establishment intact. We
245 mapped the position of Thr 278 within the Swi6-CSD relative to the dimerization interface using
246 an X-ray crystallography-based model (**Figure 3a**)[35]. The dimerization interface, consisting of
247 two helices, facilitates hydrophobic contacts between two Swi6-CSD monomers via Leu 315.
248 Disrupting the dimer by introducing a charged amino acid substitution (L315E or L315D) leads
249 to a loss of silencing *in vivo* and a loss of H3K9me binding specificity *in vitro*[35,71]. Interestingly,
250 Thr 278 lies within a beta-sheet outside the dimerization interface, with its side chain being
251 solvent-exposed. This observation supports our hypothesis that Thr 278 could be involved in
252 tuning Swi6-dependent protein-protein interactions.

253 We generated strains expressing a C-terminal V5-tagged Epe1 (Epe1-V5) to detect the
254 Swi6-Epe1 interaction using coimmunoprecipitation assays (CoIP) (**Figure 3b**). As expected,
255 Swi6-WT copurifies with Epe1-V5 from cell lysates, consistent with the two proteins directly
256 interacting *in vivo*[66]. In contrast, Swi6 is no longer detected in Epe1-V5 purifications from cells
257 expressing Swi6-Y or Swi6-K variants. This observation suggested that the Swi6-Epe1
258 interaction is disrupted in the case of both substitutions- Swi6-Y and Swi6-K irrespective of
259 whether the mutants exhibit a gain of maintenance or a loss of maintenance phenotype (**Figure**
260 **1b-c**). To further confirm that altering Thr 278 had a direct effect on Epe1 binding, we performed
261 a pulldown-based binding assay using recombinantly expressed and purified FLAG-Swi6 and
262 MBP-Epe1 (**Supplementary Figure 3a**). Consistent with our coIP results, we detected an
263 interaction between Epe1 and FLAG-Swi6-WT but not in the case of FLAG-Swi6-K *in vitro*. In
264 fact, FLAG-Swi6-K abolished Epe1 binding to a similar extent as our negative control FLAG-

265 Swi6 L315E, a mutation known to completely disrupt Swi6 dimerization and all PxVxL-
266 dependent protein interactions[44,72,73].
267 Consistent with our *ade6+* establishment phenotypes and Epe1 binding observations,
268 *swi6*-Y and *swi6*-K cells grown in -tet media also did not exhibit any additional enrichment of
269 H3K9me2 and H3K9me3 in *epe1*Δ cells compared to *epe1+* cells (**Figure 1f, 3c-d**). However,
270 H3K9me2 and H3K9me3 enrichment is selectively observed only in *swi6*-Y *epe1*Δ but not *swi6*-
271 K *epe1*Δ cells when grown in +tet media, which is fully consistent with their *ade6+* maintenance
272 phenotypes (**Figure 1f, 3c-d**).
273 To determine the molecular basis for how Swi6-Y or Swi6-K affects Epe1 binding, we used
274 AlphaFold2 Multimer (AF-M) to generate a structural model of the interaction between Epe1 and
275 Swi6[74]. First, we generated a structural prediction of the Swi6-CSD dimer. All five models
276 predicted the dimer as expected, with the highest-ranking model aligning to the published
277 crystal structures with an RMSD value of 0.49 Å (**Supplementary Figures 3b and 4**). Next, we
278 generated a structural prediction of the Swi6-CSD dimer and Epe1ΔC (amino acids 1–600),
279 which we previously showed is sufficient to strongly interact with Swi6 (**Supplementary Figure**
280 **3c**)[66]. We generated five models, all confidently predicting that Epe1ΔC binds to the Swi6
281 dimerization interface via a PxVxL-like IGVVI motif (**Supplementary Figures 3c and 5**,
282 residues 569-573). Consistent with most other variant HP1 interacting motifs, the key feature of
283 this interaction sequence is the presence of a central valine residue. In addition to this primary
284 mode of interaction, we observed a second interaction interface- namely, a predicted helix in
285 Epe1 that interacts with the auxiliary Swi6 beta-sheet surface containing Thr 278. We deleted
286 the regions of Epe1 predicted to interact with the CSD dimer (residues 566-600) to generate
287 three new alleles of Epe1 (*epe1*Δ566-600, *epe1*Δ569-573, and *epe1*Δ577-589), which harbor
288 internal deletions while the rest of the protein remains intact. Consistent with a loss of
289 interaction between Swi6 and Epe1, we observe an increase in red or sectored colonies when
290 cells were plated on +tet, consistent with increased heterochromatin maintenance much like

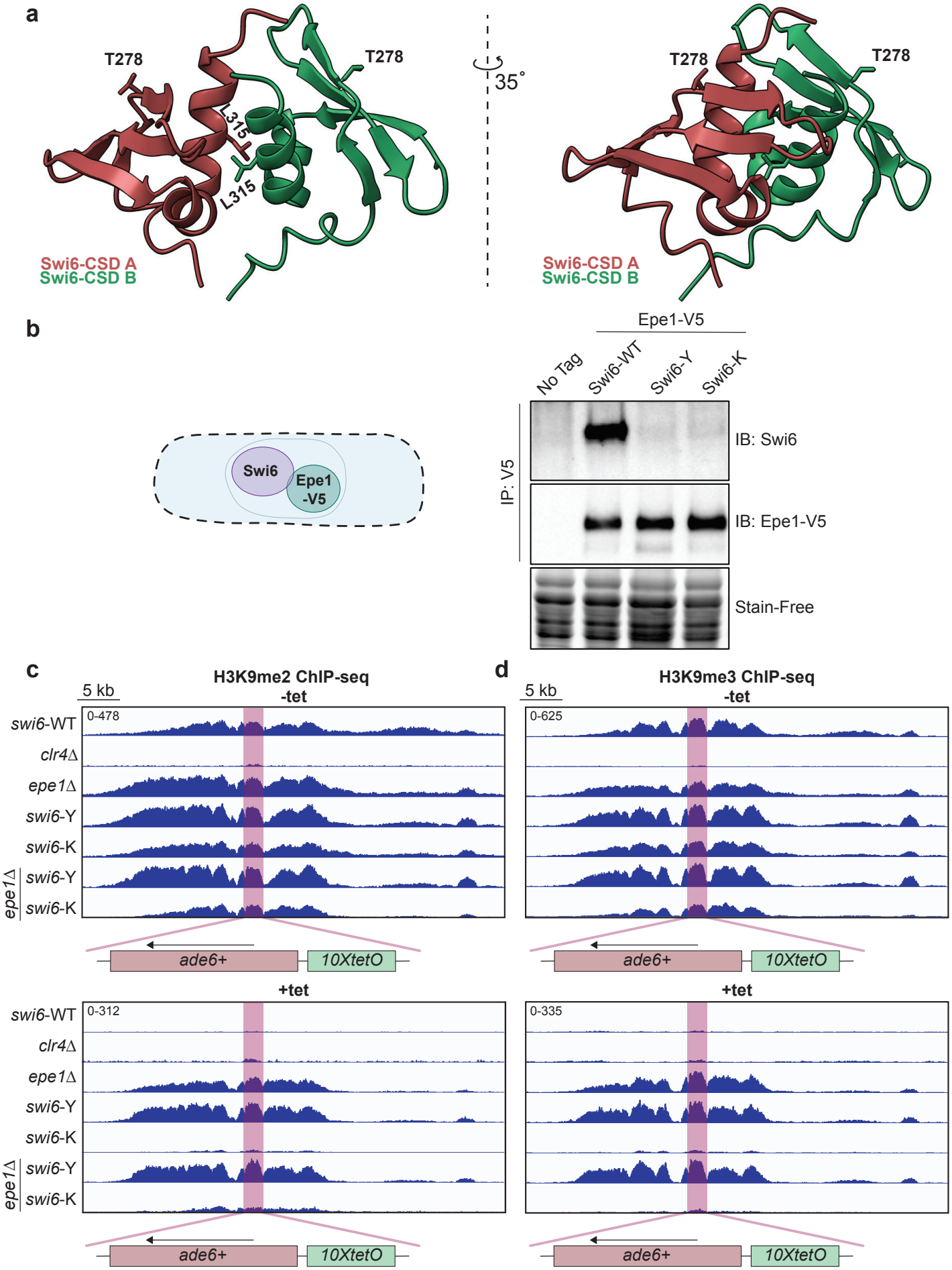

Figure 3. Swi6-Y and Swi6-K variants disrupt a direct interaction with Epe1. (**a**) X-ray crystallography structure of a Swi6-CSD dimer (PDB 1E0B, 1.90 Å). The dimerization interface and the side chains of Leu 315, a residue crucial for dimerization, are labeled. Thr 278 maps to a beta sheet interface with its side chain facing outward away from the dimerization interface. (**b**) Western blots of V5 coimmunoprecipitation (CoIP) performed with cell lysates to test the interaction between Epe1-V5 and Swi6. Epe1 is detected using a V5 antibody and Swi6 is detected using a primary antibody. (**c-d**) ChIP-seq of H3K9me2 (**c**) and H3K9me3 (**d**) surrounding the *ura4Δ::10XtetO-ade6+* reporter in indicated genotypes and tetracycline treatment. The *ura4Δ::10XtetO-ade6+* reporter is highlighted in red, displayed in a 40kb region. Enrichment in all samples is shown as normalized reads per kilobase million (RPKM).

291 what we previously observed in *epe1*Δ cells (**Supplementary Figure 3d,** *epe1*Δ566-600,
292 *epe1*Δ569-573, and *epe1*Δ577-589 *compared to swi6-WT*). Additionally, we confirmed Epe1
293 protein levels are comparable between Epe1Δ566-600, Epe1Δ569-573, Epe1Δ577-589, and full-
294 length Epe1-WT (**Supplementary Figure 3f**). To determine if the interaction with the auxiliary
295 surface where Thr 278 is embedded is generalizable, we generated a structural prediction of the
296 Swi6-CSD dimer and Sgo1, a known Swi6 interactor (**Supplementary Figures 3e and 6**)[75]. We
297 observed similar interactions in the Sgo1-Swi6 predicted structure. A helix within Sgo1, distal to
298 the PxVxL motif, interacts with the auxiliary Swi6 beta-sheet interface containing Thr 278. These
299 predictions suggest that the beta-sheet within the Swi6 CSD could serve as a novel binding site
300 outside of the dimerization interface that dictates Swi6 binding partner specificity.

301 **Swi6-Y and Swi6-K exhibit increased chromatin occupancy *in vivo*.**

302 We considered whether the molecular basis for the divergence in phenotypes between
303 Swi6-Y (gain of maintenance) and Swi6-K (loss of maintenance) might arise from biochemical
304 differences such as Swi6 dimerization or nucleosome binding. We recombinantly expressed and
305 purified different Swi6 variants (including Swi6-WT) from *E. coli* and analyzed their dimerization
306 and nucleosome binding properties *in vitro* (**Figure 4a-c, Supplementary Figures 7 and 8**). We
307 used mass photometry to measure the relative abundance of Swi6 species across a low
308 nanomolar concentration range (2.5-20 nM). Mass Photometry (MP) is a single-molecule
309 approach that uses light to detect the number and molar mass of unlabeled molecules in dilute
310 samples and, given its measurement range, we expected to detect mass differences between
311 Swi6 monomers and dimers[76]. We detected two molecular species with the predicted masses
312 for a Swi6 monomer (37 kDa) and a Swi6 dimer (74 kDa) in Swi6-WT, Swi6-Y, and Swi6-K
313 (**Supplementary Figure 7a-e**). The dimer population (74kDa) was not detected in Swi6 L315E,
314 a mutation that disrupts Swi6 dimerization (**Supplementary Figure 7c**). The observed
315 monomer-to-dimer ratios were consistent with concentration-dependent dimer formation. We
316 predominantly observed dimers at our lowest measured concentration (2.5 nM), with monomers

317 accounting for roughly 20% of the population (**Supplementary Figure 7d**). We determined
318 apparent dimerization constants using our observed relative abundance values (K_{dim},
319 **Supplementary Figure 7f**)[77]. Consistent with previous work, Swi6-WT dimerizes with an
320 apparent K_{dim} of 0.38 nM. We did not observe a significant change in dimerization affinity in
321 Swi6-Y and Swi6-K, with apparent K_{dim} values being 0.27 nM and 0.20 nM, respectively[58].
322 Although there may be modest differences in dimerization that fall outside the detection limits of
323 mass photometry, our results suggest dimerization is not significantly impacted by introducing
324 Swi6-Y or Swi6-K mutations *in vitro*.

325 To measure Swi6-nucleosome binding affinity and specificity, we performed
326 electrophoretic mobility shift assays (EMSAs) using reconstituted H3K9me0 or H3K9me3
327 mononucleosomes (**Figure 4a-c, Supplementary Figure 8)**. We observed a shift of unbound
328 nucleosomes to higher molecular weight species as Swi6 binds in a concentration-dependent
329 manner. After fitting our concentration-dependent binding assays, we determined that Swi6-WT
330 binds to H3K9me3 mononucleosomes with an apparent $K_{1/2}$ of ~50nM, which was very similar to
331 the $K_{1/2}$ for Swi6-Y binding to H3K9me3 nucleosomes (~39nM). In addition, both Swi6-WT and
332 Swi6-Y bind to H3K9me3 mononucleosomes with similar specificity (2.4-fold for Swi6-WT and
333 2.3-fold for Swi6-Y) (**Figure 4a-c**). Consistent with previous studies, we confirmed the complete
334 loss of specificity for H3K9me3 binding in control experiments measuring Swi6 L315E (**Figure**
335 **4c)**[78]. We detected no substantive differences between Swi6-WT and Swi6-Y in our *in vitro*
336 nucleosome binding assays.

337 *In vitro* binding assays using mononucleosomes do not accurately reflect how Swi6
338 binds to chromatin *in vivo*, likely due to differences in substrate length and complexity[71,79]. To
339 determine how Swi6-Y and Swi6-K bind to H3K9me in a native chromatin context, we mapped
340 the dynamics of individual Swi6 molecules in living cells (**Figure 4d**)[79]. We tracked PAmCherry-
341 Swi6-Y and PAmCherry-Swi6-K dynamics and compared them to the dynamics of PAmCherry-
342 Swi6-WT. For each mutant, we identified mobility states that best described the single-molecule

343 trajectories we measured. Each state has a defined population and an average diffusion
344 coefficient (**Figure 4e-f**)[79,80]. Swi6-WT has four mobility states, namely a fast-diffusing state
345 (unbound Swi6), a medium-diffusing state (nucleic acid-associated Swi6), a slow-diffusing state
346 (unmethylated H3K9 chromatin-associated Swi6), and a slowest-diffusing state (H3K9me2/3
347 chromatin-bound Swi6). Swi6-Y and Swi6-K exhibited only three mobility states in contrast to
348 the four states we typically observed in the case of Swi6-WT (**Figure 4e-f**). The most prominent
349 change in our mobility state measurements was a 2-fold reduction in the fraction of Swi6
350 molecules across the two variants that occupy the fast-diffusing mobility state, corresponding to
351 unbound Swi6. The medium-diffusing mobility state, corresponding to nucleic acid-associated
352 Swi6, was at the limit of our analysis and detection methods and hence not observed in either
353 Swi6-Y or Swi6-K mutants. Furthermore, the fraction of Swi6 molecules in the mobility states
354 that correspond to H3K9me chromatin-binding increased, with an estimated shift from 50% of
355 Swi6-WT molecules being chromatin-bound to ~90% of Swi6-Y and Swi6-K molecules being
356 chromatin-bound. We additionally analyzed our data using a posterior distribution analysis
357 (DPSP) to avoid overfitting biases that may arise from Bayesian methods[81]. The posterior
358 distribution analysis with DPSP revealed a greater proportion of molecules in low-mobility states
359 (chromatin-bound) with a concomitant decrease in highly mobile (free) molecules in Swi6-Y and
360 Swi6-K compared to Swi6-WT (**Figure 4g**). The DPSP analysis supports our findings of an
361 increase in the number of trajectories corresponding to low mobility molecules in Swi6-Y and
362 Swi6-K compared to Swi6-WT. Since Swi6-Y and Swi6-K have divergent maintenance
363 phenotypes, our results suggested that mechanisms other than increased chromatin occupancy
364 must contribute to the unusual maintenance phenotypes we observed.

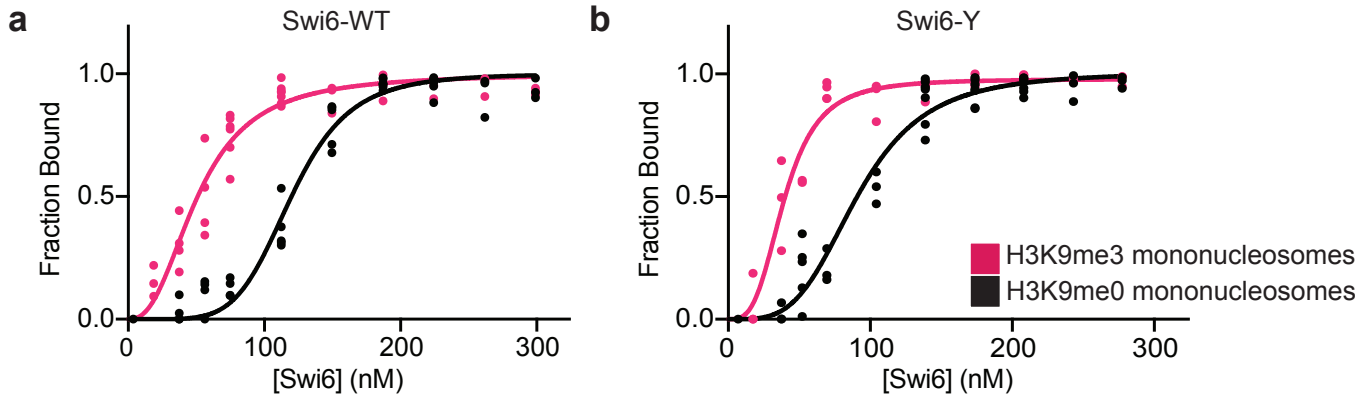

c

	$K_{1/2}$ (nM)		Specificity
	H3K9 mononucleosome	H3K9me3 mononucleosome	$K_{1/2}$ H3K9 mononucleosome / $K_{1/2}$ H3K9me3 mononucleosome
Swi6-WT	95.5 ± 3.7	42.8 ± 3.0	2.3
Swi6-Y	91.2 ± 3.2	37.7 ± 1.6	2.4
Swi6-L315E	143.1 ± 13.9	103.0 ± 3.1	1.4

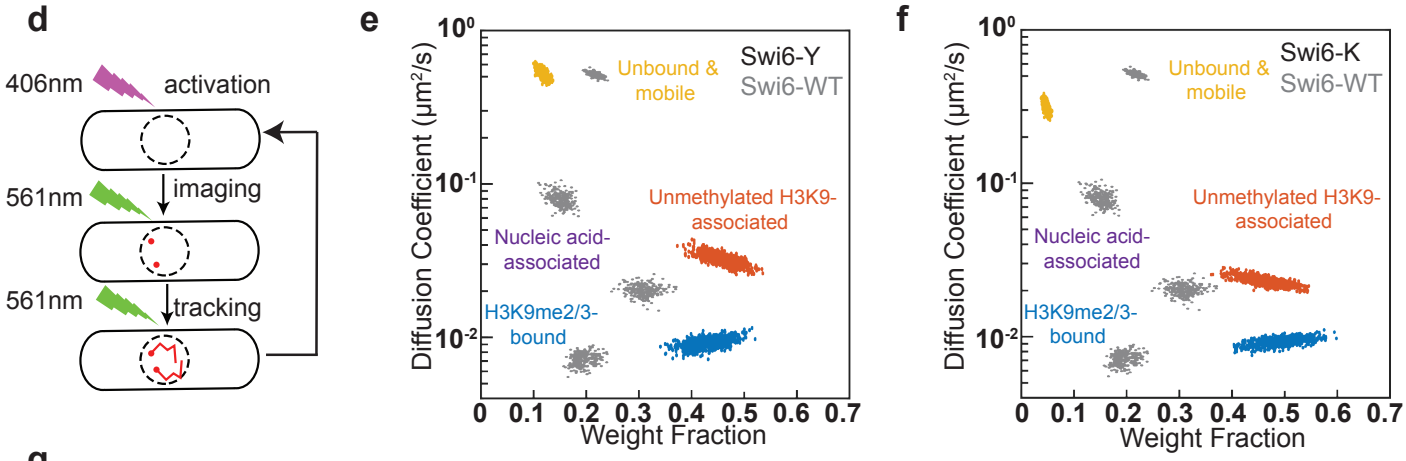

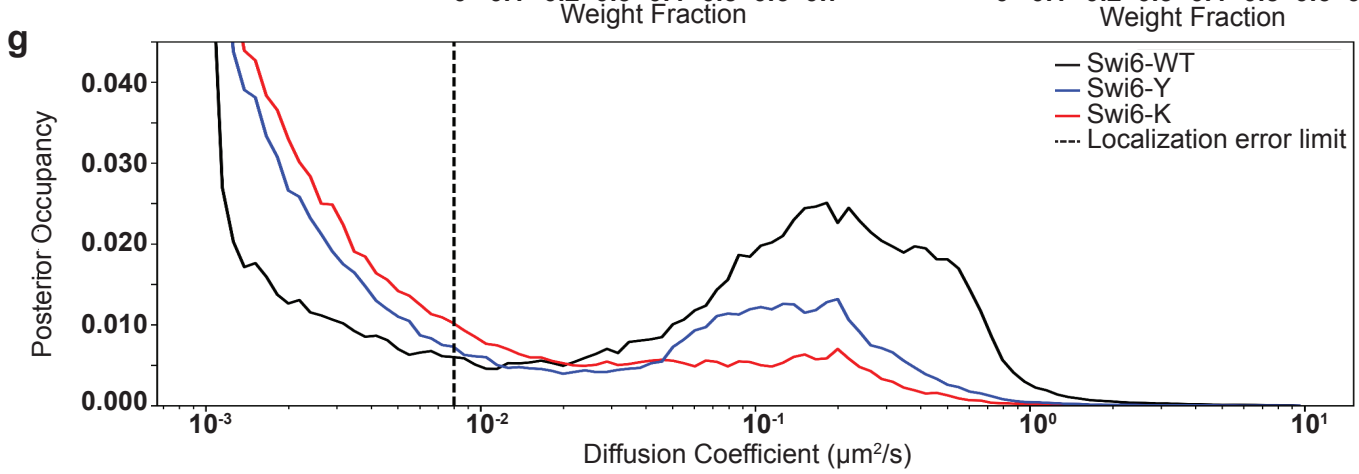

Figure 4. Swi6-Y and Swi6-K exhibit increased chromatin occupancy *in vivo*. (**a-b**) Concentration dependence curves of quantified electrophoretic mobility shift assays (EMSA) using H3K9me0 (black) and H3K9me3 (pink) mononucleosomes in (**a**) Swi6-WT and (**b**) Swi6-Y. Error bars indicate SD (N=5). (**c**) Table summarizing the apparent binding affinity (Kd) and specificity values observed for Swi6-WT, Swi6-Y and Swi6-L315E. (**d**) Schematic depicting single-molecule microscopy live-cell tracking workflow. PAmCherry-Swi6 molecules are photoactivated (406 nm) then imaged and tracked until photobleaching (561 nm, 25 frames/sec). The cycle is repeated 10 – 20 times/cell. (**e-f**) Mobility states detected by SMAUG analysis for (**e**) PAmCherry-Swi6-Y and (**f**) PAmCherry-Swi6-K. Each point is the average single-molecule diffusion coefficient of Swi6 following a single iteration of the Bayesian algorithm after convergence. Mobility states are color-coded by fast diffusing unbound state (yellow), moderately diffusing nucleic acid-associated state (purple), slow diffusing unmethylated H3K9 bound state (red), and slow diffusing H3K9me2/3 bound state (blue). Dataset: 17150 single-molecule steps from 2039 PAmCherry-Swi6-Y trajectories and 67 cells. 19718 single-molecule steps from 1225 PAmCherry-Swi6-K trajectories and 68 cells. Mobility states determined in Swi6-WT (gray) are plotted as a reference. (**g**) Posterior occupancy across diffusion coefficients for PAmCherry-Swi6-WT (black), Swi6-Y (blue), and Swi6-K (red) with DPSP analysis[81]. The dashed line represents the localization error limit separating fast diffusing molecules (right) from slow diffusing molecules (left).

365 **The Swi6-rixosome interaction modulates epigenetic inheritance.**

366 Since the loss of Epe1 binding alone cannot explain the differential maintenance
367 phenotypes we observed in Swi6-Y and Swi6-K, we investigated how all possible Swi6-
368 dependent protein interactions are affected across the two variants using quantitative mass
369 spectrometry[47,82]. We generated N-terminal FLAG-Swi6 strains to perform tandem mass tag
370 affinity purification mass spectroscopy (TMT-AP-MS, **Supplementary Figure 9a**). We compared
371 protein interactions that were significantly altered in Swi6-Y and Swi6-K relative to Swi6-WT
372 (**Figure 5a-b**). In agreement with our coIP measurements, Epe1 and its known binding partner
373 Bdf2 are downregulated ~6-fold in Swi6-Y and Swi6-K (**Figure 5a-c**)[83]. We also observed
374 selective and significant upregulation of factors with known roles in ribosomal RNA (rRNA)
375 processing, ribosome biogenesis, or nucleolar localization (~50% of all upregulated interactions)
376 in the case of Swi6-Y but not Swi6-K. Among this group are the core subunits of the conserved
377 rRNA processing and RNA degradation complex, the rixosome (**Figure 5a, c**)[21,68]. We also
378 noted a significant differential association of factors belonging to GO term categories, which
379 included heterochromatin regulation, RNA polymerase II-mediated transcription, chromatin
380 remodeling, RNA processing, DNA damage/cell cycle, and DNA replication (**Figure 5c-d**). We
381 did not observe any significant changes in interactions with heterochromatin-associated factors
382 that have known functions in epigenetic inheritance, which include subunits of the H3K9
383 methyltransferase CLRC complex, a deacetylase-remodeler complex, SHREC, the histone
384 chaperone complex. FACT, nuclear pore complex subunits, and the nucleosome remodeler,
385 Ino80 complex across both Swi6 variants (**Supplementary Figure 9b**)[21,47,84-87].

386 Our quantitative mass spectrometry results suggested that the gain-of-maintenance
387 phenotype we observed in Swi6-Y was determined by the extent of its interaction with subunits
388 of the rixosome complex. To test this hypothesis, we generated a separation-of-function
389 mutation in the Grc3 subunit of the rixosome (*grc3* V70M). This mutation disrupts the rixosome-
390 Swi6 interaction without affecting its ribosome biogenesis functions[68]. *swi6*-Y *grc3* V70M cells

exhibited red colonies in -tet media, consistent with successful heterochromatin establishment. However, cells plated on +tet media turned white, consistent with a loss of *ade6+* silencing and selective disruption of maintenance (**Figure 5e**). Therefore, the enhanced maintenance phenotype in the case of Swi6-Y is critically dependent on its specific interaction with the rixosome complex.

Our mass spectrometry data provided a straightforward explanation for enhanced maintenance in the case of Swi6-Y. However, the molecular basis of Swi6-K defective maintenance remains unclear. We considered the possibility that a change in rixosome binding in Swi6-K is either too small for sensitive detection using mass spectrometry or that these changes correspond only to the rixosome chromatin bound fraction. To test this, we fused the Crb3 subunit of the rixosome with a C-terminal TAP tag and performed ChIP-qPCR to measure its occupancy at the pericentromeric repeats (*dg*) and the *10XtetO-ade6+* reporter locus (*SPCC.330.06c*) (**Figure 5f**). We detected a small but significant decrease in rixosome binding at both loci in Swi6-K relative to Swi6-WT. Consistent with our mass spectrometry findings, we observe a significant increase in rixosome binding at the pericentromeric repeats and reporter gene locus in Swi6-Y. These results suggest that the persistent loss of maintenance observed in Swi6-K is likely due to reduced rixosome binding at heterochromatin (**Figure 5f**). These observations also explain why deleting Epe1 cannot rescue the maintenance defect in Swi6-K (**Figure 1f**).

We generated a model of the Swi6-CSD dimer and Grc3 using AF-M (**Supplementary Figure 9c**). Grc3 interacts with the Swi6-CSD dimer using a PxVxL-like motif, but the upstream and downstream contacts between Grc3 and the Swi6-CSD are strikingly different compared to what we previously observed in the case of Sgo1 and Epe1 (**Supplementary Figure 3c, f**). The helix that we previously noted in our Epe1-Swi6 and Sgo1-Swi6 structural models interacting with the Swi6 auxiliary surface containing Thr 278 was notably absent in all five Grc3-Swi6 models (**Supplementary Figure 10**). These *in silico* differences across Swi6 binding partners

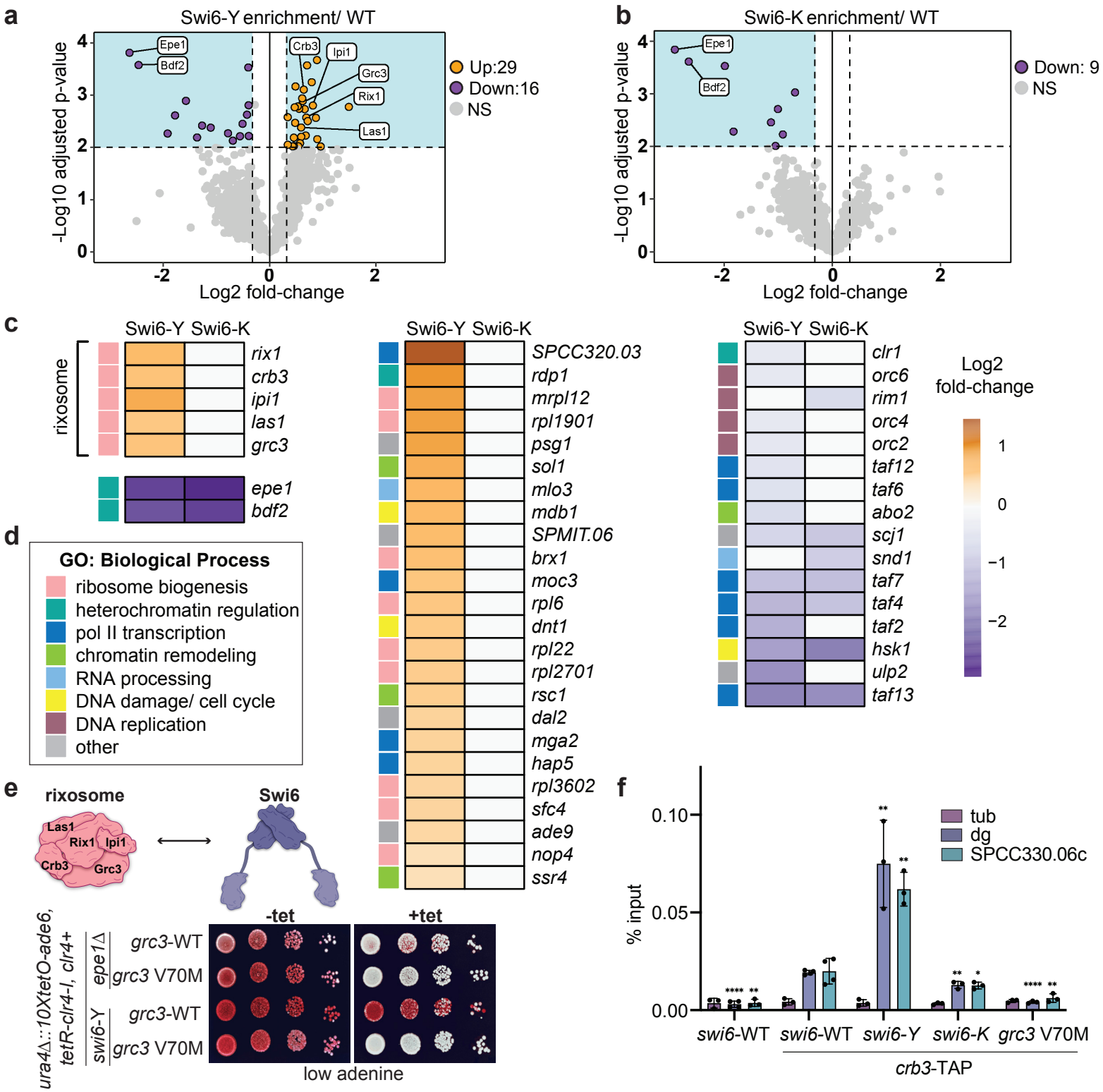

Figure 5. The Swi6-rixosome interaction modulates epigenetic inheritance. (**a-b**) Volcano plot displaying the results from tandem mass tag mass spectrometry (TMT-MS) of affinity purifications of (**a**) 3XFLAG-Swi6-Y and (**b**) 3XFLAG-Swi6-K. Samples were normalized to untagged Swi6 and plotted against the reference (3XFLAG-Swi6-WT). The shaded boxes mark a p-value = 0.01 (horizontal) and a 1.25-fold enrichment over the 3XFLAG-Swi6-WT reference (vertical) (N = 3), only interactions detected with > 1 peptide are included in the dataset. Proteins are color-coded as upregulated interactions (orange), downregulated interactions (purple), unenriched interactions (grey), and relevant heterochromatin regulators are labeled. The full dataset of interacting proteins can be found in Table S1. (**c**) Heat map comparing upregulated (orange) and downregulated (purple) interactions observed in Swi6-Y and Swi6-K, p-value cutoff is < 0.01. (**d**) GO term analysis of biological process categories for upregulated and downregulated interactions. Each interaction within the (C) heat map is annotated with a colored box, denoting its corresponding GO-term biological process. The sample size for each GO term is as follows: ribosome biogenesis N = 14, heterochromatin regulation N = 4, pol II transcription N = 10, chromatin remodeling N = 4, RNA processing N = 2, DNA damage/ cell cycle N = 3, DNA replication N = 4, other N = 6. (**e**) Top- Schematic of the rixosome complex subunits. Bottom- Silencing assay of *ura4Δ::10XtetO-ade6+* reporter in indicated genotypes in the absence (-tet) and presence (+tet) of tetracycline. Red cells indicate ade6+ silencing. Cells are plated at 10-fold serial dilutions. (**f**) ChIP-qPCR measuring Crb3-TAP at *tub*, *dg*, and *SPCC330.06c* in indicated genotypes. Error bars indicate SD (N=3 or N=4, replicates plotted for each sample). Mean of each sample were compared to their corresponding swi6-WT mean using an unpaired one-tailed t-test (P value cutoff < 0.05) and the significance values are represented as follows P < 0.05 (*), P < 0.01 (**), P < 0.0001 (****).

417 (Grc3, Sgo1, and Epe1) could provide a potential molecular basis for tunability that depends on
418 interactions with an auxiliary binding surface that extends beyond the dimerization interface.

419 **Genetic rescue of Swi6-K heterochromatin maintenance defects**

420 Previous work has shown that targeting the histone deacetylase Clr3 to heterochromatin
421 (either by tethering Clr3 or by fusing chromodomains) is sufficient for epigenetic inheritance
422 despite the presence of Epe1[66,85]. The HDAC activity of Clr3 reduces histone turnover, a
423 characteristic feature of heterochromatin that is thought to promote epigenetic inheritance[88]. We
424 wanted to test if tethering Clr3 is sufficient to rescue defective maintenance in *swi6*-K
425 expressing cells. We expressed a Gal4-Clr3 fusion protein in strains containing two orthogonal
426 DNA binding sequences, i.e. *10XUAS* sites for Gal4 binding and *10XtetO* sites for TetR binding-
427 both of which are placed upstream of the *ade6+* reporter gene (**Supplementary Figure 11a**).
428 Despite Epe1 being present, we observed robust maintenance of *ade6+* silencing, with cells
429 appearing red or sectored when plated on +tet media (**Supplementary Figure 11a**, *swi6*-WT*,*
430 *gal4-clr3*). This process is critically dependent on Swi6 since both establishment and
431 maintenance were eliminated in cells lacking Swi6 (**Supplementary Figure 11a**, *swi6*Δ, *gal4-*
432 *clr3*). Interestingly, tethering Clr3 rescued the Swi6-K maintenance defect since we observed
433 both successful establishment (red colonies, -tet) and maintenance (red or sectored colonies in
434 +tet), although maintenance was not nearly as robust as what we observed in *swi6*-WT cells
435 (**Supplementary Figure 11a**). Furthermore, targeting Clr3 could not bypass the requirement for
436 the rixosome interaction in heterochromatin maintenance. In cells expressing *grc3*-V70M,
437 tethering Clr3 failed to produce red or sectored colonies when cells were plated on +tet-
438 containing medium (**Supplementary Figure 11a**). Hence, Clr3-mediated histone deacetylation
439 can compensate for defective heterochromatin maintenance in the case of *swi6*-K but not in the
440 case of *grc3*-V70M.

441 We envisioned that an alternative approach to detect the molecular basis for defective
442 maintenance in Swi6-K cells would be to identify other residues in Swi6 that could suppress this

443 defect. These compensatory mutations could potentially restore protein interactions that are lost
444 in Swi6-K cells. To identify such mutations, we utilized a PCR based targeted saturation
445 mutagenesis approach as previously described (**Supplementary Figure 1a**) to generate a
446 library of variants in residues that are proximal to Swi6-K (residues: 268-277, 279-302). This
447 screen revealed substitutions at D283 to histidine (H), threonine (T), serine (S), arginine (R),
448 and glutamic acid (E) that could rescue the maintenance defect in the Swi6-K background,
449 indicated by red or sectored colonies on YE+tet plates (**Supplementary Figure 11b**). This
450 residue, D283, falls within a region of Swi6 involved in binding to the histone chaperone
451 complex, FACT[87]. Collectively, our observations suggest that the Swi6-K maintenance defect is
452 likely mediated by changes in protein interactions, correlated with decreased rixosome binding.

453 **DISCUSSION**

454 HP1 proteins have a conserved architecture yet are functionally versatile[32]. We
455 hypothesized that regions which exhibit high sequence variability within the otherwise
456 conserved chromoshadow domain (CSD) could contribute towards HP1 proteins acquiring novel
457 functional properties. To test this hypothesis, we used a targeted mutagenesis screen of the
458 Swi6-CSD to identify new variants that exhibit enhanced heterochromatin maintenance. We
459 have demonstrated that substitutions associated with a single amino-acid residue, Thr 278,
460 within the Swi6-CSD can influence the maintenance of an ectopic heterochromatin domain while
461 preserving Swi6 dimerization, nucleosome binding, and transcriptional silencing. Our findings
462 support a model where sequence variation outside the dimerization interface can enable Swi6,
463 and possibly other HP1 proteins, to acquire new functional attributes. Hence, the plasticity of
464 HP1 proteins arises not from changes to conserved sites but from alterations within auxiliary
465 regions that preserve overall protein architecture. *In silico* modeling of Epe1, Sgo1, and Grc3,
466 with the Swi6-CSD dimer reveals minimal differences in how the PxVxL motif (or PxVxL variant
467 motifs) bind to the Swi6-CSD dimer interface[44,89]. In contrast, our predictions show significant
468 divergence in motifs that may interact with the Thr 278-containing beta-sheet interface

469 (**Supplementary Figures 3c, 3e, and 9c**). Although further validation is required to understand
470 the structural implications of our generated models, our studies potentially reveal a new
471 interface in an HP1 protein that determines protein binding specificity.

472 Although structural studies to support our AF-M models are currently unavailable, NMR
473 measurements have identified interactions between peptides of Clr3, Sgo1, and histone H2B
474 with the Swi6-CSD dimer[40,58]. These data also identified potential interactions involving Thr 278
475 and other neighboring residues within Swi6[40,58]. Therefore, our experimental findings are
476 consistent with a model where Thr 278 can function as a specificity determinant, thus enabling
477 Swi6 to differentiate between protein interactors, all of which share a PxVxL-like motif and bind
478 to a common Swi6-CSD interface. The importance of Thr 278 in altering Swi6 function is also
479 underscored by a screen for G0 suppressors, which previously identified Swi6 T278K (or Swi6-
480 K) as a mutation that promotes the survival of fission yeast cells following quiescence[90]. Hence,
481 the interface we identified likely contributes to heterochromatin maintenance in G2 cells but may
482 have other classes of interactors that depend on Swi6 during quiescence.

483 Previous studies identified HP1 mutations associated with the N-terminal chromodomain
484 (CD) which affects H3K9me binding and oligomerization or the C-terminal chromoshadow
485 domain (CSD) mutants that disrupt dimerization[44,71,75,78,91,92]. Since dimerization is crucial for
486 HP1-dependent protein-protein interactions, it is nearly impossible to introduce mutations within
487 the dimerization interface without compromising its overall structure and function. The variants
488 we identified in our study map to an auxiliary surface outside the CSD dimerization interface.
489 This enables selective tuning of protein-protein interactions without disrupting overall Swi6
490 function, especially in the context of heterochromatin establishment. While we have shown how
491 the Epe1-rixosome-Swi6 axis is sensitive to substitutions within the auxiliary beta sheet binding
492 interface, other studies have shown that the histone chaperone complex FACT, which directly
493 binds to Swi6, is insensitive to mutations within this interface. In agreement with our proteomics
494 data, Thr 278 substitutions (Swi6 T278K and T278A) do not alter the interaction between Swi6

495 and Spt16[87]. Furthermore, recent work has shown that the Drosophila HP1 protein Rhino
496 utilizes its chromodomain to interact with the transcription factor Kipferl[93]. Moreover, mutations
497 affecting Kipferl binding do not affect H3K9me recognition, suggesting this interface can also
498 potentially be exploited for evolving new protein-protein interactions[94].

499 We aligned HP1 sequences across the *Schizosaccharomyces* lineage (*S.cryophilus,*
500 *S.japonicus, S.octosporus,* and *S.osmophilus*) and found minimal sequence variation within the
501 auxiliary beta-sheet region across Swi6 orthologs (**Supplementary Figure 12**). However,
502 sequence conservation within this region significantly declines when comparing Swi6 to Chp2 or
503 HP1 proteins from other organisms[44,53]. Hence, in addition to variations within PxVxL motif
504 binding, we propose that the auxiliary beta sheet we identified can further contribute to
505 functional divergence between HP1 proteins[46]. The lineage and variant-specific conservation of
506 this region have important consequences for envisioning what the "ground state" of
507 heterochromatin systems might be in different organisms. Most substitutions, apart from the
508 original Thr 278 residue, led to the persistent gain of epigenetic inheritance, and a subset of
509 charged amino acid substitutions led to a persistent loss of epigenetic inheritance (**Figure 1b-c**).
510 Both extreme scenarios' consequences are absolute, with heterochromatin being inflexible and
511 not regulatable. Therefore, our findings suggest Thr 278 and other proximal amino acid residues
512 within the beta-sheet interface in Swi6 and other HP1 proteins contribute to epigenetic plasticity
513 wherein cells can invoke memory depending on changes in their physiology or environment.

514 Consistent with this model, there are proposed mechanisms for regulating Swi6 protein
515 interactions that may contribute to epigenetic plasticity. Notably, heterochromatin maintenance
516 in *S. pombe* is responsive to environmental changes, which can be regulated by altering Epe1
517 availability in cells. Epe1 expression is sensitive to glucose availability, cAMP levels, stress, and
518 ubiquitination[95-99]. Furthermore, post-translational modifications of Swi6, such as
519 phosphorylation, can alter the balance of interactions between the histone deacetylase Clr3 and

520 H3K9 demethylase Epe1. The loss of Swi6 phosphorylation leads to increased Epe1
521 interactions and decreased heterochromatin silencing[70].
522 The divergent phenotypes associated with Swi6-Y and Swi6-K present an interesting
523 case study for how minimal changes within an HP1 protein, where protein architecture is
524 preserved, can serve as drivers of functional innovation. It is evident from our biochemistry and
525 mass spectrometry data that these divergent effects are not due to differences in protein
526 structure (Swi6-Y and Swi6-K form stable dimers), nucleosome binding (site-specific
527 perturbations do not affect H3K9me binding), or interactions with Epe1. Furthermore, both
528 variants exhibit increased chromatin occupancy *in vivo* yet produce opposite effects on
529 epigenetic inheritance. Our findings demonstrate that simply increasing Swi6 occupancy on
530 chromatin is insufficient to induce epigenetic inheritance. Instead, the primary deciding factor for
531 epigenetic inheritance in *S. pombe* is the extent to which H3K9me bound Swi6 efficiently
532 interacts with components of the rixosome complex and recruits them to heterochromatin[21,68].
533 We have previously shown that substitution mutations, which are thought to affect Epe1
534 catalytic activity, lead to a loss of a direct interaction between Epe1 and Swi6[66]. The trade-off in
535 protein-protein interactions that we observed in the case of Swi6-Y lends additional support to a
536 model where Epe1 regulates epigenetic inheritance by attenuating the interaction between Swi6
537 and heterochromatin maintenance enhancers such as the rixosome (**Figure 6**). Our findings
538 suggest that the molecular basis for the loss of maintenance in the case of Swi6-K is likely also
539 mediated by changes in protein-protein interactions. We can rescue the maintenance defect
540 observed in Swi6-K two ways: through D283 compensatory mutations or by tethering Clr3 at the
541 ectopic locus (**Supplementary Figure 11**). Given D283 has been previously implicated in FACT
542 complex binding, our findings suggest these compensatory D283 (H,T, R, S and E) substitutions
543 may lead to a gain in FACT binding[87]. Additionally, Clr3 tethering has been shown to bypass
544 essential factors in heterochromatin inheritance, including the rescue of reduced H3K9me
545 density, increased histone turnover, and impaired heterochromatin positioning at the nuclear

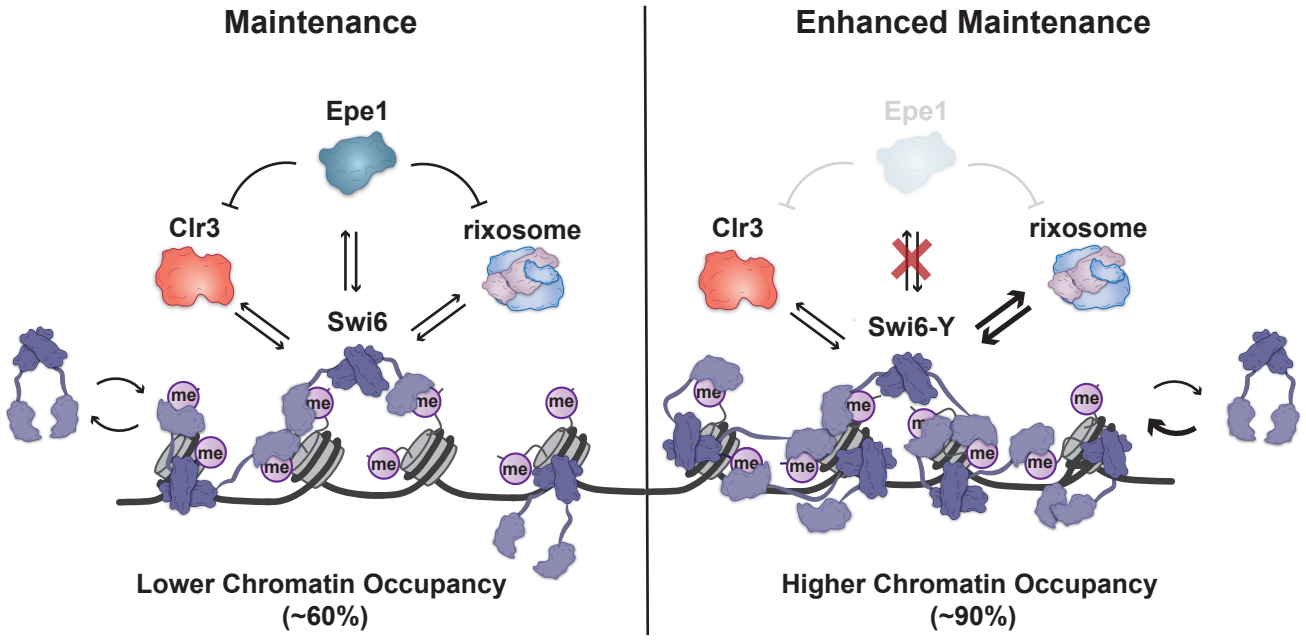

Figure 6. Model for Swi6-CSD-mediated epigenetic inheritance capacity. The CSD amino acid composition in Swi6-WT permits binding to effector proteins that inhibit (Epe1) and promote (Clr3 and rixosome) heterochromatin, leading to restriction of heterochromatin maintenance at the ectopic locus. Upon Swi6-Y mutation, the Epe1 interaction is lost and the rixosome interaction is upregulated, leading to enhanced heterochromatin maintenance. Upon Swi6-K mutation, the Epe1 interaction is lost but the rixosome interaction is not upregulated, leading to defective heterochromatin maintenance. Swi6-Y and Swi6-K are more chromatin-bound than Swi6-WT, indicating the chromatin landscape is altered. The rixosome is recruited to heterochromatin directly by Swi6 for heterochromatin RNA clearance. Chromatin-associated transcripts are processed for subsequent degradation, allowing for Clr4-mediated read-write heterochromatin inheritance. Therefore, our findings support a model where Swi6-mediated effector recruitment, specifically Epe1 and the rixosome, influences epigenetic inheritance of heterochromatin.

546 periphery[85]. Therefore, the increased recruitment of "maintenance factors" such as Clr3 or FACT
547 can rescue the defective maintenance in Swi6-K cells. Despite Clr3 having multifaceted rescue
548 effects on heterochromatin, we could not restore maintenance in a *grc3* V70M background by
549 tethering Clr3 (**Supplementary Figure 11a**). Therefore, unlike many other essential
550 maintenance regulators, the requirement for the rixosome cannot be bypassed by Clr3 during
551 heterochromatin maintenance, which strongly suggests that the rixosome acts downstream of
552 Clr3-mediated histone deacetylation.

553 Our observations support a model where the basic unit of epigenetic inheritance must
554 involve multiprotein, Swi6-dependent complexes that assemble using H3K9me chromatin as a
555 template[24]. This model is consistent both with the Swi6-Y variant having increased chromatin
556 occupancy and increased interactions with heterochromatin maintenance enhancers such as
557 the rixosome. We envision that the stable association of Swi6 before and after DNA replication
558 could have a crucial role in ensuring that epigenetic states remain stable and heritable across
559 multiple generations. It is possible to envision a scenario where Swi6 binds to H3K9me
560 heterochromatin, and the protein-protein interaction network that emerges from this binding
561 makes its inheritance unique and distinct from euchromatin[6].

562 **METHODS**

563 **Strains**

564 All mutation, deletion, and tagging strains were generated using published standard
565 protocols, which include PCR-based gene targeting, the SpEDIT CRISPR/Cas9 system, or by a
566 cross followed by random spore analysis[100-102]. All strains used in this study are listed in
567 Supplementary Table 1.

568 **Site-directed saturation mutagenesis library generation**

569 The site-directed saturation mutagenesis is adapted from[103]. Primers were designed to
570 contain an "NNN" degenerate sequence at every codon position within the Swi6 coding
571 sequence and were commercially synthesized. A Swi6 plasmid template was generated using
572 topoisomerase-based cloning. The insert sequence was generated by PCR from genomic DNA
573 and included the Swi6 coding sequence with 500-bp flanking homology segments. The library
574 was generated by three-step PCR. The first PCR reaction introduces the degenerate codons,
575 the second extends the truncated PCR products from step 1, and the third adds the necessary
576 homology for recombination at the endogenous Swi6 locus. The library was transformed into a
577 strain where the endogenous Swi6-CSD is deleted with a ura4-kan selection marker. Positive
578 transformants were selected by growth on FOA and loss of G418 resistance. Red or pink
579 colonies on YE (establishment) were subsequently tested on YE+tet (maintenance). Colonies
580 that show maintenance were considered library hits, and the Swi6 mutation was mapped using
581 Sanger sequencing.

582 **Expression and Purification of Recombinant Protein**

583 Swi6 expression and purification approach was adapted based on an earlier study[79].
584 Swi6 coding sequence was cloned into N-terminal 6XHis-tag–containing pET vectors, and
585 mutants were generated using site-directed mutagenesis. All Swi6 proteins were purified from
586 BL21(DE3)-RIPL *E. coli* cells. Cells were grown at 37°C to OD 0.5 to 0.8 in LB media with
587 ampicillin (100 µg/ml), induced with 0.4 mM isopropyl-β-D-thiogalactopyranoside (IPTG), and

were grown for 16 hours at 18°C. Cells were harvested and resuspended in lysis buffer [1× phosphate-buffered saline (PBS) buffer (pH 7.3), 300 mM NaCl, 10% glycerol, 0.1% Igepal CA-630, 1 mM phenylmethylsulfonyl fluoride (PMSF), aprotonin (1 µg/ml), pepstatin A, and leupeptin] and sonicated. Cell debris was removed by centrifugation at 25,000*g* for 35 min. Cell lysates were incubated with HisPur NiNTA resin (Thermo Fisher Scientific) at 4°C for at least 2 hours. The resin was washed with lysis buffer, and protein was eluted [20 mM Hepes (pH 7.5), 100 mM KCl, 10% glycerol, and 500 mM imidazole] and incubated with the corresponding protease (Ulp1 or TEV) overnight at 4°C. After cleavage of 6XHis-tag, the products were further isolated by anion exchange chromatography using a HiTRAP Q HP column (Cytiva) and size exclusion chromatography using a Superdex200 10/300 (Cytiva) column. Proteins were dialyzed into storage buffer [20 mM Hepes, 100 mM KCl, 10% glycerol, and 1 mM dithiothreitol (DTT)]. Protein concentrations were determined using ultraviolet (UV) absorption measurements at 280 nm and molecular weights (MWs) and extinction coefficients computationally determined for Swi6-WT (MW = 37,292.6 g/mol, ε = 41,035 M^{-1} cm^{-1}), Swi6-L315E (MW = 37,308.6 g/mol, ε = 41,035 M^{-1} cm^{-1}), Swi6-T278Y (MW = 37,354.7 g/mol, ε = 42,525 M^{-1} cm^{-1}), and Swi6-T278K (MW = 37,319.7 g/mol, ε = 41,035 M^{-1} cm^{-1}) using the Expasy ProtParam tool. Protein was further equalized using SDS-PAGE densitometry quantification. Epe1 was purified as described previously [66]. MBP-His-TEV-Epe1 was cloned into a pFastBac vector (Thermo Fisher Scientific) and used for Bacmid generation. Low-titer baculoviruses were produced by transfecting Bacmid into Sf21 cells using Cellfectin II reagent (Gibco). Full-length *S. pombe* Epe1 protein (wild-type and mutant) was expressed in Hi5 cells infected by high titer baculovirus, amplified from Sf21 cells. After 44 h of infection, Hi5 cells were harvested and lysed in buffer A (30 mM Tris-HCl (pH 8.0), 500 mM NaCl, 5 mM EDTA, 5 mM β-mercaptoethanol with protease inhibitor cocktails) using Emulsiflex-C3 (Avestin). The cleared cell lysate was applied to Amylose resin (New England Biolabs), followed by washing with buffer A and elution with buffer A containing 10 mM maltose. Proteins were further purified using a Superdex 200 (GE Healthcare) size exclusion

column. The protein was concentrated in a storage buffer containing 30 mM Tris-HCl (pH 8.0), 500 mM NaCl, 30% glycerol, and 1 mM TCEP.

Total protein extraction from *S. pombe*

To detect protein expression in strains containing Swi6 mutants and tagged proteins, protein extracts were prepared using Trichloroacetic Acid (TCA) precipitation. Strains were grown in liquid yeast extract supplemented with adenine (YEA) for 16 hours at 32°C, and 7 ODs worth of cells were harvested. Cell pellets were washed with 1 mL of ice-cold water and resuspended in 150 µL of YEX Buffer (1.85 M NaOH, 7.5% beta-mercaptoethanol). After 10 minutes of incubation on ice, protein precipitation was performed by adding 150 µL of 50% TCA (~3 N) and mixing by inversion. The extracts were then incubated for 10 minutes on ice, pelleted by centrifugation, and excess TCA was carefully removed. The protein extracts were resuspended in 2X SDS sample buffer (125 mM Tris-Base pH 6.8, 8M urea, 5% SDS, 20% glycerol, 5% BME) and centrifuged for 5 minutes to clear cell debris. Samples were analyzed by western blotting, as described below.

Western Blotting

Protein samples were resolved by gel electrophoresis on 4–20% Mini-PROTEAN® TGX Stain-Free™ Protein Gels. Immunoblotting was performed using the BioRad Trans-Blot Turbo Transfer System, and transfer was performed at 2.5A and 25V for 7 minutes onto 0.2 µm Nitrocellulose. Membranes were blocked using 5% non-fat dry milk in Tris-buffered saline pH 7.5 with 0.1% Tween-20 (TBST) for 1 hour. The membrane was then incubated with the primary antibody at an optimized concentration overnight at 4°C. Following incubation, the membrane was washed 3 times with TBST and incubated with the appropriate secondary antibody for 1 hour at room temperature. After the incubation, the membrane was washed 3 times with TBST and incubated with SuperSignal West Pico/Femto PLUS Chemiluminescent Substrate. The membrane was imaged for chemiluminescence on a Bio-Rad ChemiDoc. For quantitative Swi6

639 western, an Alexa Fluor 647 conjugated secondary antibody (A-21246, Invitrogen) was used
640 and imaged using the Alexa Fluor 647 filter on a BioRad ChemiDoc.

641 **Coimmunoprecipitation to detect Epe1-Swi6 interaction**

642 CoIP experiments were performed as described previously[66]. 1.5 L of fission yeast cells
643 were grown in YEA medium at 32°C to an OD_{600} = 3.5 and harvested by centrifugation. The cell
644 pellets were washed with 10 ml TBS pH 7.5, resuspended in 1.5 ml lysis buffer (30 mM HEPES
645 pH 7.5, 100 mM NaCl, 0.25% Triton X-100, 5 mM $MgCl_{2,}$1 mM DTT), and the cell suspension
646 was snap-frozen into liquid nitrogen drop-wise and cryogenically ground using a SPEX 6875D
647 Freezer Mill. The frozen cell powder was stored at -80˚C, thawed at room temperature, and
648 resuspended in an additional 10 ml of lysis buffer with a protease inhibitor cocktail and 1 mM
649 PMSF. Cell lysates were subjected to two rounds of centrifugation at 18000 rpm for 5 and 30
650 mins in a JA-25.50 rotor (Beckman). Protein levels were normalized for coimmunoprecipitation
651 and immunoblot analysis using a Bradford Assay. Protein G Magnetic Beads were pre-
652 incubated with V5 antibody (A01724, Genscript) for 4 h and crosslinked with 10 volumes of
653 crosslinking buffer containing 20 mM DMP (3 mg DMP/ml of 0.2 M Boric Acid pH 9) for 30 min
654 at room temperature by rotating. Crosslinking was quenched by washing twice and incubated
655 with 0.2 M ethanolamine pH 8 for 2 h at room temperature. The cell lysates were then incubated
656 with antibody crosslinked beads for 3 h at 4°C. Beads were washed thrice in 1 ml lysis buffer for
657 5 mins each, then eluted with 500 µl of 10 mM ammonium hydroxide. The ammonium hydroxide
658 was evaporated using a speed vac (SPC-100H) for 5 h and resuspended in SDS sample buffer.
659 Samples were resolved using SDS–polyacrylamide gel electrophoresis (SDS-PAGE) and
660 transferred to PVDF membranes. Immunoblotting was performed by blocking the PVDF
661 membrane in Tris-buffered saline (TBS) pH 7.5 with 0.1% Tween-20 (TBST) containing 5% non-
662 fat dry milk and subsequently probed with desired primary antibodies and secondary antibodies.
663 Blots were developed by enhanced chemiluminescence (ECL) method and detected using a
664 Bio-Rad ChemiDoc Imaging System.

665 ***In vitro* binding assay to detect Epe1-Swi6 interaction**

666 *In vitro* binding assays were performed by immobilizing recombinant 3X FLAG-Swi6 on
667 25 µl of FLAG M2 beads, which were incubated with three different concentrations of
668 recombinant MBP-Epe1 fusion proteins in 600 µl binding buffer containing 20 mM HEPES pH
669 7.5, 150 mM NaCl, 5 mM $MgCl_2$, 10% glycerol, 0.25% Triton -X 100, 1 mM DTT. Reactions were
670 incubated at 4°C for 2 h and washed three times in 1 ml washing buffer (20 mM HEPES pH 7.5,
671 150 mM NaCl, 5 mM $MgCl_2$, 10% glycerol, 0.25% Triton -X 100, 1 mM DTT) for 5 min each, then
672 30µl of SDS sample buffer was added followed by incubation at 95°C for 5 min. Proteins were
673 separated through SDS-PAGE and transferred to a PVDF membrane followed by incubation
674 with anti-MBP monoclonal antibody (E8032S, NEB) and M2 Flag antibody (A8592, Sigma).
675 Western blot data for *in vitro* binding assays were analyzed using ImageJ software. The
676 exposure times for the interaction assays were chosen and differed in each experiment to
677 capture differences in the interaction between Epe1 and Swi6 depending on the assay
678 conditions. Assays performed on different blots cannot be compared, but samples loaded on the
679 same blot can be readily compared.

680 **Tandem-mass tag affinity purification mass spec**

681 Protein levels were normalized between the triplicate samples by silver stain. Dried
682 eluates were sent to the Thermo Fisher Center for Multiplexed Proteomics at Harvard Medical
683 School for further processing and analysis. Dried samples were resuspended in 20 mM EPPS,
684 pH 8.5. Samples were reduced with TCEP, alkylated with iodoacetamide, and further reduced
685 with DTT. Proteins were extracted with SP3 beads. Samples were digested overnight at room
686 temperature with Lys-C, followed by digestion with trypsin for 6 hours at 37˚C. Protein samples
687 were labeled with TMTPro reagents, and complete labeling was confirmed. All samples were
688 pooled and desalted by stage-tip. Peptides were analyzed on an Orbitrap Eclipse Mass
689 Spectrometer. MS2 spectra were searched using the COMET algorithm against an *S. pombe*
690 Uniprot composite database (downloaded in 2023) containing its reversed complement and

691 known contaminants. For proteome, Peptide spectral matches were filtered to a 1% false
692 discovery rate (FDR) using the target-decoy strategy combined with linear discriminant analysis.
693 The proteins were filtered to a <1% FDR and quantified only from peptides with a summed SN
694 threshold of >120.

695 **Silencing Assays**

696 Cells were grown in 3 ml of yeast extract containing adenine (YEA) at 32°C overnight.
697 Cells were washed twice in water and then resuspended to a concentration of `~10^7 cells/ml.
698 Ten-fold serial dilutions (~5μL) were plated on YE plates to evaluate establishment and
699 YE+AHT to evaluate maintenance. Plates were incubated for 2-3 days before the results were
700 cataloged.

701 **Chromatin immunoprecipitation (ChIP)**

702 For H3K9me2 and H3K9me3 ChIP, 30 ml of cells were grown to late log phase (OD_{600}-
703 1.8-2.2) in yeast extract supplemented with adenine (YEA) or YEA containing tetracycline (2.5
704 μg/ml) and fixed with 1% formaldehyde for 15 min at room temperature (RT). For TAP ChIP, 25
705 ml of cells were grown to late log phase (OD_{600}-1.8-2.2) in yeast extract supplemented with
706 adenine (YEA) or YEA containing tetracycline (2.5 μg/ml) and then grown for 2 hrs at 18˚C.
707 Cells were crosslinked with 1.5 mM ethylene glycol bis(succinimidyl succinate) (EGS) for 30 min
708 at RT and then 1% formaldehyde for 30 min. 130 mM glycine was added to quench the reaction
709 and incubated for 5 min at RT. The cells were harvested by centrifugation and washed with TBS
710 (50 mM Tris, pH 7.6, 500 mM NaCl). Cell pellets were resuspended in 300 μL lysis buffer (50
711 mM HEPES-KOH, pH 7.5, 100 mM NaCl, 1mM EDTA, 1% Triton X-100, 0.1% SDS, and
712 protease inhibitors) to which 500 μL 0.5 mm glass beads were added. Cell lysis was carried out
713 by bead beating using Omni Bead Ruptor at 3000 rpm x 30sec x 10 cycles. Tubes were
714 punctured, and the flow-through was collected in a new tube by centrifugation, which was
715 subjected to sonication to obtain fragment sizes of roughly 100-500 bp long. After sonication,
716 the extract was centrifuged for 15 min at 13000 rpm at 4°C. The soluble chromatin was

717 transferred to a fresh tube and normalized for protein concentration by Bradford assay. For each
718 normalized sample, 25 µL lysate was saved as input, to which 225 µL of 1xTE/1% SDS were
719 added (TE: 50 mM Tris pH 8.0, 1 mM EDTA). Protein A Dynabeads were preincubated with
720 H3K9me2 antibody (Abcam, ab1220) or H3K9me3 antibody (39161, Active Motif). For each
721 immunoprecipitation, we used 2 µg H3K9me2 antibody (Abcam, ab1220) and 2 µg H3K9me3
722 antibody (39161, Active Motif). For TAP ChIP, Dynabeads Pan Mouse IgG (Invitrogen, 11042)
723 were used. Samples were incubated for 3h at 4°C. The beads were collected on magnetic
724 stands and washed 3 times with 1 mL lysis buffer and once with 1 mL TE. For eluting bound
725 chromatin, 100 µL elution buffer I (50 mM Tris pH 8.0, 10 mM EDTA, 1% SDS) was added, and
726 the samples were incubated at 65°C for 5 min. The eluate was collected and incubated with 150
727 µL 1xTE/0.67% SDS in the same way. Input and immunoprecipitated samples were incubated
728 overnight at 65°C to reverse crosslink. 60 µg glycogen, 100 µg proteinase K (Roche), 44 µL of
729 5M LiCl, and 250 µL of 1xTE were added to each sample, and incubation was continued at
730 55°C for 1h. Phenol/chloroform extraction was carried out for all the samples, followed by
731 ethanol precipitation. Immuno-precipitated DNA was resuspended in 100 µL of 10 mM Tris pH
732 7.5 and 50 mM NaCl. ChIP experiments were analyzed using quantitative PCR with Taq
733 polymerase and SYBR Green using a CFX Opus 384 Real-Time PCR System. PCR primers are
734 listed in Supplementary Table 2.

735 **ChIP-Seq library preparation and processing**

736 ChIP-seq libraries were prepared and processed as described previously[25]. Libraries
737 were constructed using the manufacturer's guidelines in the NEBNext® Ultra™ II FS DNA
738 Library Prep Kit for Illumina, using 1ng of starting material. Barcoded libraries were pooled and
739 sequenced with next-generation sequencing. First, raw reads were demultiplexed by barcode.
740 Then, the sequences were trimmed with Trimmomatic, aligned with BWA, and normalized by
741 reads per million [104,105]. The reads were visualized with IGV.

742 **RNA extraction**

743 10 mL of cells were grown to late log phase (OD_{600}-1.8-2.2) in yeast extract
744 supplemented with adenine. Cells were resuspended in 750 µL TES buffer (0.01 M Tris pH7.5,
745 0.01 M EDTA, 0.5% SDS). Immediately, 750 µL of acidic phenol-chloroform was added and
746 vortexed for 2 minutes. Samples were incubated at 65°C for 40 minutes while vortexing for 20
747 seconds every ten minutes. The aqueous phase was separated by centrifuging in Phase Lock
748 tubes for 5 minutes at 13000 rpm at 4°C. The aqueous phase was transferred to new tubes, and
749 ethanol precipitated. After extraction, RNA was treated with DNase. Then, the RNA was cleaned
750 using RNeasy Mini kits (Qiagen). cDNA was prepared using oligodT and SuperScript III
751 Reverse Transcriptase (Invitrogen). The cDNA was then used for qPCR with SYBR Green and
752 Taq polymerase on a CFX OPUS 384 Real-Time PCR System. RNA levels were quantified
753 using ΔC_T compared to tubulin *(tub1*) RNA levels. PCR primers are listed in Supplementary
754 Table 2.

755 **Mass Photometry**

756 All mass photometry experiments were performed using full-length recombinant Swi6
757 protein at the Center for Macromolecular Interactions at Harvard Medical School using a Refeyn
758 TwoMP instrument. Before taking measurements, the instrument was calibrated using a protein
759 standard containing 10 nM β-amylase (Sigma Aldrich A8781) and 3 nM Thyroglobulin (Sigma-
760 Aldrich 609310). Swi6 proteins were diluted to 100 nM in 20 mM HEPES pH 7.5, 100 mM KCl
761 immediately before taking measurements. For each measurement, the objective was focused
762 using 20 mM HEPES pH 7.5, 100 mM KCl, and the corresponding volume of 100 nM Swi6 was
763 added to the droplet to achieve the desired final concentration (2.5-20 nM). Sample data was
764 collected immediately. Figures and Gaussian fits of the resulting data were generated using the
765 Refeyn DiscoverMP software. Apparent dimerization constants (K_{dim}) were determined by
766 relative molecular abundance of the monomer and dimer populations at known Swi6
767 concentrations[77,106].

768 **AlphaFold2-multimer (AF-M) structural prediction**

769 AlphaFold2 Multimer was used to predict protein-protein interactions using the Cosmic[2]
770 Science Gateway server[74,107]. In all cases, we obtained 5 models with 3 recycles, and all
771 structures were unrelaxed. Protein structures were plotted using Chimera[108]. We further
772 analyzed our structures using a published pipeline to determine interface statistics from
773 predicted multimer structural models[109]. This pipeline identifies all interchain interactions within 8
774 angstroms across all five models. The pipeline also provides several metrics to score the
775 confidence of the predicted multimer interfaces accounting for the consistency of interactions
776 and pLDDT scores across all models (**Supplementary Figures 4f, 5f, 6f, 10f**).

777 ***S. pombe* live-cell imaging**

778 Yeast strains containing a copy of PAmCherry-Swi6 or a PAmCherry-Swi6 mutant under
779 the control of the native Swi6 promoter were grown in standard complete YES media (US
780 Biological, catalog no. Y2060) containing the full complement of yeast amino acids and
781 incubated overnight at 32°C. This initial culture was diluted and incubated at 25°C with shaking
782 to reach an optical density at 600 nm (OD_{600}) of ~0.5. To maintain cells in an exponential phase
783 and eliminate extranuclear vacuole formation, the culture was maintained at OD_{600} ~0.5 for 2
784 days, diluting at ~12-hour intervals. To prepare agarose pads for imaging, cells were pipetted
785 onto a pad of 2% agarose prepared in YES media with 0.1 mM *N*-propyl gallate (Sigma-Aldrich,
786 catalog no. P-3130) and 1% gelatin (Millipore, catalog no. 04055) as additives to reduce
787 phototoxicity during imaging. *S. pombe* cells were imaged at room temperature with a 100x 1.40
788 numerical aperture (NA) oil-immersion objective in an Olympus IX-71 inverted microscope. First,
789 the fluorescent background was decreased by exposure to 488 nm light (Coherent Sapphire,
790 200 W/cm^2 for 20 to 40 s). A 406-nm laser (Coherent Cube, 405-100; 102 W/cm^2) was used for
791 photoactivation (200-ms activation time), and a 561-nm laser (Coherent Sapphire, 561-50; 163
792 W/cm^2) was used for imaging. Images were acquired at 40-ms exposure time per frame. The
793 fluorescence emission was filtered with a Semrock LL02-561-12.5 long-pass filter and a Chroma

794 ZT488/561rpc 488/561 dichroic mirror to eliminate the 561 nm excitation source and imaged
795 using a 512 × 512-pixel Photometrics Evolve EMCCD camera.

796 **Single-molecule trajectory analysis**

797 Recorded Swi6-PAmCherry single-molecule positions were detected and localized with
798 two-dimensional Gaussian fitting with home-built MATLAB software as previously described and
799 connected into trajectories using the Hungarian algorithm[110-112]. These single-molecule trajectory
800 datasets were analyzed by a nonparametric Bayesian framework to reveal heterogeneous
801 dynamics [80]. This SMAUG algorithm uses nonparametric Bayesian statistics and Gibbs
802 sampling to identify the number of distinct mobility states in the single molecule tracking dataset
803 in an iterative manner. It also infers parameters, including weight fraction and average apparent
804 diffusion coefficient for each mobility state, assuming a Brownian motion model. To ensure that
805 even rare events were captured, we collected more than 10,000 steps in our single-molecule
806 tracking dataset for each measured strain, and we ran the algorithm over >10,000 iterations to
807 achieve a thoroughly mixed state space. The state number and associated parameters were
808 updated in each iteration of the SMAUG algorithm and saved after convergence. The final
809 estimation shows the data after convergence for iterations with the most frequent state number.
810 Each mobility state is assigned a distinct color, and for each saved iteration, the average
811 diffusion coefficient of that state is plotted against the weight fraction. The distributions of
812 estimates over the iterations give the uncertainty in the determination of the parameters. For
813 measurement of static molecules in fixed *S. pombe* cells, SMAUG converges to a single state
814 with D_{avg} = 0.0041 ± 0.0003 μm^2/s. The average localization error for single-molecule
815 localizations in this fixed-cell imaging is 32.6 nm. To benchmark against a model that overcomes
816 potential overfitting of the Bayesian model, we also applied the DPSP package to acquire the
817 posterior occupancy distribution for diffusion coefficients of Swi6 and variants [81]. The DPSP
818 package uses a Dirichlet process mixture model to acquire the posterior probability distribution
819 for each dataset. The same trajectory datasets used in SMAUG analysis were stored in csv

format and analyzed with the Python package DPSP under default parameter settings and corresponding pixel size and frame interval (https://github.com/alecheckert/dpsp).

Nucleosome Electrophoretic Mobility Shift Assays (EMSAs)

Samples were prepared by varying concentrations of Swi6 while keeping substrate concentration, i.e. 10 nM mononucleosomes (H3K9me0 and H3K9me3, Epicypher catalog nos. 16-0006 and 16-0315-20) constant in binding buffer [20 mM Hepes (pH 7.5), 4 mM tris, 80 mM KCl, 0.1% Igepal CA-630, 0.2 mM EDTA, 2 mM DTT, and 10% glycerol]. Samples were incubated at 30°C for 45 min. A 0.5x tris-borate EDTA 6% acrylamide:bis-acrylamide 37.5:1 gel was pre-run at RT for at least 1 hour at 75 V. Reactions were loaded on the gel and ran under the same conditions for 3 hours. Gels were poststained for 2 hours with polyacrylamide gel electrophoresis (PAGE) GelRed DNA stain (Biotium) and imaged using a Typhoon Imager. The unbound nucleosome band was quantified using ImageJ, and binding curves were fit using nonlinear regression (Prism 9).

DATA AVAILABILITY

Sequencing data has been deposited in GEO under accession code GSE248428. The mass spectrometry proteomics data have been deposited to the ProteomeXchange Consortium via the PRIDE partner repository with the dataset identifier PXD047651[113,114]. Source data are provided with this paper.

ACKNOWLEDGMENTS

The authors declare no competing interests. We thank Danesh Moazed for sharing the fission yeast strains used in this study. We thank Saarang Gopinath for his support in obtaining preliminary data during the initial phase of this study. This work was supported by the National Science Foundation (grant no. EF-2316281 to K.R. and J.S.B), National Institutes of Health (grant nos. R35GM137832 to K.R.; T32GM007544 to A.A and A.L.; and T32GM007315 to M.S) and American Cancer Society (grant no. RSG-22-117-01-DMC to K.R.) Molecular graphics and analyses were performed with UCSF Chimera, developed by the Resource for Biocomputing,

846 Visualization, and Informatics at the University of California, San Francisco, with support from
847 NIH P41-GM103311. AlphaFold-Multimer-based *in silico* models were generated using
848 Cosmic2[107]. We thank the Center for Macromolecular Interactions at Harvard Medical School
849 and the Thermo Fisher Scientific Center for Multiplex Proteomics at Harvard Medical School for
850 their support.

851 **AUTHOR CONTRIBUTIONS**

852 A.A. and K.R. developed the concept, designed the study, interpreted the findings, and prepared
853 the manuscript. A.A., M.S., A. Larkin, G.R., Z.C., and A. Levashkevich. performed experimental
854 studies and analysis. B.K. contributed to experimental studies. M.S., A. Larkin, G.R., Z.C., A.
855 Levashkevich, and J.S.B. provided technical support, conceptual advice, and edited the
856 manuscript.

REFERENCES

1 Misteli, T. The Self-Organizing Genome: Principles of Genome Architecture and Function. *Cell* **183**, 28-45, doi:10.1016/j.cell.2020.09.014 (2020).

2 Allfrey, V. G., Faulkner, R. & Mirsky, A. E. Acetylation and methylation of histones and their possible role in the regulation of RNA synthesis. *Proc Natl Acad Sci U S A* **51**, 786-794, doi:10.1073/pnas.51.5.786 (1964).

3 Hildebrand, E. M. & Dekker, J. Mechanisms and Functions of Chromosome Compartmentalization. *Trends in Biochemical Sciences* **45**, 385-396, doi:10.1016/j.tibs.2020.01.002 (2020).

4 Rea, S. *et al.* Regulation of chromatin structure by site-specific histone H3 methyltransferases. *Nature* **406**, 593-599, doi:10.1038/35020506 (2000).

5 Ringrose, L., Ehret, H. & Paro, R. Distinct contributions of histone H3 lysine 9 and 27 methylation to locus-specific stability of polycomb complexes. *Mol Cell* **16**, 641-653, doi:10.1016/j.molcel.2004.10.015 (2004).

6 Reinberg, D. & Vales, L. D. Chromatin domains rich in inheritance. *Science* **361**, 33-34, doi:10.1126/science.aat7871 (2018).

7 Hanahan, D. & Weinberg, Robert A. Hallmarks of Cancer: The Next Generation. *Cell* **144**, 646-674, doi:10.1016/j.cell.2011.02.013 (2011).

8 Flavahan, W. A., Gaskell, E. & Bernstein, B. E. Epigenetic plasticity and the hallmarks of cancer. *Science* **357**, doi:10.1126/science.aal2380 (2017).

9 Moazed, D. Mechanisms for the inheritance of chromatin states. *Cell* **146**, 510-518, doi:10.1016/j.cell.2011.07.013 (2011).

10 Xu, M. *et al.* Partitioning of Histone H3-H4 Tetramers During DNA Replication–Dependent Chromatin Assembly. *Science* **328**, 94-98, doi:10.1126/science.1178994 (2010).

11 Yu, C. *et al.* A mechanism for preventing asymmetric histone segregation onto replicating DNA strands. *Science* **361**, 1386-1389, doi:10.1126/science.aat8849 (2018).

12 Petryk, N. *et al.* MCM2 promotes symmetric inheritance of modified histones during DNA replication. *Science* **361**, 1389-1392, doi:10.1126/science.aau0294 (2018).

13 Nathanailidou, P. *et al.* Specialized replication of heterochromatin domains ensures self-templated chromatin assembly and epigenetic inheritance. *Proceedings of the National Academy of Sciences* **121**, e2315596121, doi:doi:10.1073/pnas.2315596121 (2024).

14 Stewart-Morgan, K. R., Petryk, N. & Groth, A. Chromatin replication and epigenetic cell memory. *Nature Cell Biology* **22**, 361-371, doi:10.1038/s41556-020-0487-y (2020).

15 Audergon, P. N. C. B. *et al.* Restricted epigenetic inheritance of H3K9 methylation. *Science* **348**, 132-135, doi:doi:10.1126/science.1260638 (2015).

16 Zhang, K., Mosch, K., Fischle, W. & Grewal, S. I. Roles of the Clr4 methyltransferase complex in nucleation, spreading and maintenance of heterochromatin. *Nat Struct Mol Biol* **15**, 381-388, doi:10.1038/nsmb.1406 (2008).

17 Uckelmann, M. & Davidovich, C. Not just a writer: PRC2 as a chromatin reader. *Biochem Soc Trans* **49**, 1159-1170, doi:10.1042/bst20200728 (2021).

18 Ragunathan, K., Jih, G. & Moazed, D. Epigenetic inheritance uncoupled from sequence-specific recruitment. *Science* **348**, 1258699, doi:doi:10.1126/science.1258699 (2015).

19 Brickner, J. H. Inheritance of epigenetic transcriptional memory through read–write replication of a histone modification. *Annals of the New York Academy of Sciences* **1526**, 50-58, doi:https://doi.org/10.1111/nyas.15033 (2023).

20 Owen, J. A., Osmanović, D. & Mirny, L. Design principles of 3D epigenetic memory systems. *Science* **382**, eadg3053, doi:doi:10.1126/science.adg3053 (2023).

21 Holla, S. *et al.* Positioning Heterochromatin at the Nuclear Periphery Suppresses Histone Turnover to Promote Epigenetic Inheritance. *Cell* **180**, 150-164.e115, doi:https://doi.org/10.1016/j.cell.2019.12.004 (2020).
22 Francis, N. J., Follmer, N. E., Simon, M. D., Aghia, G. & Butler, J. D. Polycomb proteins remain bound to chromatin and DNA during DNA replication in vitro. *Cell* **137**, 110-122, doi:10.1016/j.cell.2009.02.017 (2009).
23 Eeftens, J. M., Kapoor, M., Michieletto, D. & Brangwynne, C. P. Polycomb condensates can promote epigenetic marks but are not required for sustained chromatin compaction. *Nature Communications* **12**, doi:10.1038/s41467-021-26147-5 (2021).
24 Nakayama, J.-i., Klar, A. J. S. & Grewal, S. I. S. A Chromodomain Protein, Swi6, Performs Imprinting Functions in Fission Yeast during Mitosis and Meiosis. *Cell* **101**, 307-317, doi:10.1016/S0092-8674(00)80840-5 (2000).
25 Seman, M., Levashkevich, A., Larkin, A., Huang, F. & Ragunathan, K. Uncoupling the distinct functions of HP1 proteins during heterochromatin establishment and maintenance. *Cell Reports* **42**, doi:10.1016/j.celrep.2023.113428 (2023).
26 Lee, S. *et al.* Intrinsic mesoscale properties of a Polycomb protein underpin heterochromatin fidelity. *Nat Struct Mol Biol* **30**, 891-901, doi:10.1038/s41594-023-01000-z (2023).
27 Strahl, B. D. & Allis, C. D. The language of covalent histone modifications. *Nature* **403**, 41-45, doi:10.1038/47412 (2000).
28 Yun, M., Wu, J., Workman, J. L. & Li, B. Readers of histone modifications. *Cell Res* **21**, 564-578, doi:10.1038/cr.2011.42 (2011).
29 Vakoc, C. R., Mandat, S. A., Olenchock, B. A. & Blobel, G. A. Histone H3 lysine 9 methylation and HP1gamma are associated with transcription elongation through mammalian chromatin. *Mol Cell* **19**, 381-391, doi:10.1016/j.molcel.2005.06.011 (2005).
30 Sanchez, R. & Zhou, M. M. The PHD finger: a versatile epigenome reader. *Trends Biochem Sci* **36**, 364-372, doi:10.1016/j.tibs.2011.03.005 (2011).
31 Lu, R. & Wang, G. G. Tudor: a versatile family of histone methylation 'readers'. *Trends Biochem Sci* **38**, 546-555, doi:10.1016/j.tibs.2013.08.002 (2013).
32 Canzio, D., Larson, A. & Narlikar, G. J. Mechanisms of functional promiscuity by HP1 proteins. *Trends in Cell Biology* **24**, 377-386, doi:https://doi.org/10.1016/j.tcb.2014.01.002 (2014).
33 Franklin, K. A., Shields, C. E. & Haynes, K. A. Beyond the marks: reader-effectors as drivers of epigenetics and chromatin engineering. *Trends Biochem Sci* **47**, 417-432, doi:10.1016/j.tibs.2022.03.002 (2022).
34 James, T. C. & Elgin, S. C. R. Identification of a Nonhistone Chromosomal Protein Associated with Heterochromatin in Drosophila melanogaster and Its Gene. *Molecular and Cellular Biology* **6**, 3862-3872, doi:10.1128/mcb.6.11.3862-3872.1986 (2023).
35 Cowieson, N. P., Partridge, J. F., Allshire, R. C. & McLaughlin, P. J. Dimerisation of a chromo shadow domain and distinctions from the chromodomain as revealed by structural analysis. *Current Biology* **10**, 517-525, doi:https://doi.org/10.1016/S0960-9822(00)00467-X (2000).
36 Bannister, A. J. *et al.* Selective recognition of methylated lysine 9 on histone H3 by the HP1 chromo domain. *Nature* **410**, 120-124, doi:10.1038/35065138 (2001).
37 Strom, A. R. *et al.* Phase separation drives heterochromatin domain formation. *Nature* **547**, 241-245, doi:10.1038/nature22989 (2017).
38 Larson, A. G. *et al.* Liquid droplet formation by HP1α suggests a role for phase separation in heterochromatin. *Nature* **547**, 236-240, doi:10.1038/nature22822 (2017).
39 Yamada, T., Fukuda, R., Himeno, M. & Sugimoto, K. Functional domain structure of human heterochromatin protein HP1(Hsalpha): involvement of internal DNA-binding and

C-terminal self-association domains in the formation of discrete dots in interphase nuclei. *J Biochem* **125**, 832-837, doi:10.1093/oxfordjournals.jbchem.a022356 (1999).
40 Sanulli, S. *et al.* HP1 reshapes nucleosome core to promote phase separation of heterochromatin. *Nature* **575**, 390-394, doi:10.1038/s41586-019-1669-2 (2019).
41 Larson, A. G. & Narlikar, G. J. The Role of Phase Separation in Heterochromatin Formation, Function, and Regulation. *Biochemistry* **57**, 2540-2548, doi:10.1021/acs.biochem.8b00401 (2018).
42 Zhang, H., Qin, W., Romero, H., Leonhardt, H. & Cardoso, M. C. Heterochromatin organization and phase separation. *Nucleus* **14**, 2159142, doi:10.1080/19491034.2022.2159142 (2023).
43 Smothers, J. F. & Henikoff, S. The HP1 chromo shadow domain binds a consensus peptide pentamer. *Curr Biol* **10**, 27-30, doi:10.1016/s0960-9822(99)00260-2 (2000).
44 Thiru, A. *et al.* Structural basis of HP1/PXVXL motif peptide interactions and HP1 localisation to heterochromatin. *Embo j* **23**, 489-499, doi:10.1038/sj.emboj.7600088 (2004).
45 Stephens, G. E., Slawson, E. E., Craig, C. A. & Elgin, S. C. Interaction of heterochromatin protein 2 with HP1 defines a novel HP1-binding domain. *Biochemistry* **44**, 13394-13403, doi:10.1021/bi051006+ (2005).
46 Leopold, K., Stirpe, A. & Schalch, T. Transcriptional gene silencing requires dedicated interaction between HP1 protein Chp2 and chromatin remodeler Mit1. *Genes & Development* **33**, 565-577, doi:10.1101/gad.320440.118 (2019).
47 Iglesias, N. *et al.* Native Chromatin Proteomics Reveals a Role for Specific Nucleoporins in Heterochromatin Organization and Maintenance. *Molecular Cell* **77**, 51-66.e58, doi:10.1016/j.molcel.2019.10.018 (2020).
48 Liu, Y. *et al.* Peptide recognition by heterochromatin protein 1 (HP1) chromoshadow domains revisited: Plasticity in the pseudosymmetric histone binding site of human HP1. *J Biol Chem* **292**, 5655-5664, doi:10.1074/jbc.M116.768374 (2017).
49 Levine, M. T. *et al.* Phylogenomic Analysis Reveals Dynamic Evolutionary History of the Drosophila Heterochromatin Protein 1 (HP1) Gene Family. *PLOS Genetics* **8**, e1002729, doi:10.1371/journal.pgen.1002729 (2012).
50 Helleu, Q. & Levine, M. T. Recurrent Amplification of the Heterochromatin Protein 1 (HP1) Gene Family across Diptera. *Mol Biol Evol* **35**, 2375-2389, doi:10.1093/molbev/msy128 (2018).
51 Hiragami-Hamada, K. *et al.* N-terminal phosphorylation of HP1{alpha} promotes its chromatin binding. *Mol Cell Biol* **31**, 1186-1200, doi:10.1128/mcb.01012-10 (2011).
52 Mendez, D. L. *et al.* The HP1a disordered C terminus and chromo shadow domain cooperate to select target peptide partners. *Chembiochem* **12**, 1084-1096, doi:10.1002/cbic.201000598 (2011).
53 Mendez, D. L., Mandt, R. E. & Elgin, S. C. R. Heterochromatin Protein 1a (HP1a) Partner Specificity Is Determined by Critical Amino Acids in the Chromo Shadow Domain and C-terminal Extension *. *Journal of Biological Chemistry* **288**, 22315-22323, doi:10.1074/jbc.M113.468413 (2013).
54 Allshire, R. C. & Ekwall, K. Epigenetic Regulation of Chromatin States in Schizosaccharomyces pombe. *Cold Spring Harb Perspect Biol* **7**, a018770, doi:10.1101/cshperspect.a018770 (2015).
55 Ivanova, A. V., Bonaduce, M. J., Ivanov, S. V. & Klar, A. J. S. The chromo and SET domains of the Clr4 protein are essential for silencing in fission yeast. *Nature Genetics* **19**, 192-195, doi:10.1038/566 (1998).
56 Thon, G. & Verhein-Hansen, J. Four Chromo-domain Proteins of Schizosaccharomyces pombe Differentially Repress Transcription at Various Chromosomal Locations. *Genetics* **155**, 551-568, doi:10.1093/genetics/155.2.551 (2000).

57 Sadaie, M. *et al.* Balance between Distinct HP1 Family Proteins Controls Heterochromatin Assembly in Fission Yeast. *Molecular and Cellular Biology* **28**, 6973-6988, doi:10.1128/MCB.00791-08 (2008).
58 Isaac, R. S. *et al.* Biochemical Basis for Distinct Roles of the Heterochromatin Proteins Swi6 and Chp2. *J Mol Biol* **429**, 3666-3677, doi:10.1016/j.jmb.2017.09.012 (2017).
59 Motamedi, M. R. *et al.* HP1 Proteins Form Distinct Complexes and Mediate Heterochromatic Gene Silencing by Nonoverlapping Mechanisms. *Molecular Cell* **32**, 778-790, doi:10.1016/j.molcel.2008.10.026 (2008).
60 Sadaie, M. *et al.* Balance between Distinct HP1 Family Proteins Controls Heterochromatin Assembly in Fission Yeast. *Molecular and Cellular Biology* **28**, 6973-6988, doi:10.1128/mcb.00791-08 (2023).
61 Hayashi, A. *et al.* Heterochromatin protein 1 homologue Swi6 acts in concert with Ers1 to regulate RNAi-directed heterochromatin assembly. *Proceedings of the National Academy of Sciences* **109**, 6159-6164, doi:10.1073/pnas.1116972109 (2012).
62 Rougemaille, M. *et al.* Ers1 links HP1 to RNAi. *Proceedings of the National Academy of Sciences* **109**, 11258-11263, doi:10.1073/pnas.1204947109 (2012).
63 Yamada, T., Fischle, W., Sugiyama, T., Allis, C. D. & Grewal, S. I. S. The Nucleation and Maintenance of Heterochromatin by a Histone Deacetylase in Fission Yeast. *Molecular Cell* **20**, 173-185, doi:10.1016/j.molcel.2005.10.002 (2005).
64 Zofall, M. & Grewal, S. I. S. Swi6/HP1 Recruits a JmjC Domain Protein to Facilitate Transcription of Heterochromatic Repeats. *Molecular Cell* **22**, 681-692, doi:10.1016/j.molcel.2006.05.010 (2006).
65 Fischer, T. *et al.* Diverse roles of HP1 proteins in heterochromatin assembly and functions in fission yeast. *Proceedings of the National Academy of Sciences* **106**, 8998-9003, doi:10.1073/pnas.0813063106 (2009).
66 Raiymbek, G. *et al.* An H3K9 methylation-dependent protein interaction regulates the non-enzymatic functions of a putative histone demethylase. *eLife* **9**, e53155, doi:10.7554/eLife.53155 (2020).
67 Garcia, J. F., Dumesic, P. A., Hartley, P. D., El-Samad, H. & Madhani, H. D. Combinatorial, site-specific requirement for heterochromatic silencing factors in the elimination of nucleosome-free regions. *Genes & Development* **24**, 1758-1771, doi:10.1101/gad.1946410 (2010).
68 Shipkovenska, G., Durango, A., Kalocsay, M., Gygi, S. P. & Moazed, D. A conserved RNA degradation complex required for spreading and epigenetic inheritance of heterochromatin. *Elife* **9**, doi:10.7554/eLife.54341 (2020).
69 Allshire, R. C., Javerzat, J. P., Redhead, N. J. & Cranston, G. Position effect variegation at fission yeast centromeres. *Cell* **76**, 157-169, doi:10.1016/0092-8674(94)90180-5 (1994).
70 Shimada, A. *et al.* Phosphorylation of Swi6/HP1 regulates transcriptional gene silencing at heterochromatin. *Genes & Development* **23**, 18-23, doi:10.1101/gad.1708009 (2009).
71 Canzio, D. *et al.* Chromodomain-mediated oligomerization of HP1 suggests a nucleosome-bridging mechanism for heterochromatin assembly. *Mol Cell* **41**, 67-81, doi:10.1016/j.molcel.2010.12.016 (2011).
72 Brasher, S. V. *et al.* The structure of mouse HP1 suggests a unique mode of single peptide recognition by the shadow chromo domain dimer. *The EMBO Journal* **19**, 1587-1597, doi:https://doi.org/10.1093/emboj/19.7.1587 (2000).
73 Haldar, S., Saini, A., Nanda, J. S., Saini, S. & Singh, J. Role of Swi6/HP1 self-association-mediated recruitment of Clr4/Suv39 in establishment and maintenance of heterochromatin in fission yeast. *J Biol Chem* **286**, 9308-9320, doi:10.1074/jbc.M110.143198 (2011).

74 Evans, R. *et al.* Protein complex prediction with AlphaFold-Multimer. *bioRxiv*, doi:10.1101/2021.10.04.463034 (2022).
75 Yamagishi, Y., Sakuno, T., Shimura, M. & Watanabe, Y. Heterochromatin links to centromeric protection by recruiting shugoshin. *Nature* **455**, 251-255, doi:10.1038/nature07217 (2008).
76 Asor, R. & Kukura, P. Characterising biomolecular interactions and dynamics with mass photometry. *Current Opinion in Chemical Biology* **68**, 102132, doi:https://doi.org/10.1016/j.cbpa.2022.102132 (2022).
77 Soltermann, F. *et al.* Quantifying Protein-Protein Interactions by Molecular Counting with Mass Photometry. *Angew Chem Int Ed Engl* **59**, 10774-10779, doi:10.1002/anie.202001578 (2020).
78 Canzio, D. *et al.* A conformational switch in HP1 releases auto-inhibition to drive heterochromatin assembly. *Nature* **496**, 377-381, doi:10.1038/nature12032 (2013).
79 Biswas, S. *et al.* HP1 oligomerization compensates for low-affinity H3K9me recognition and provides a tunable mechanism for heterochromatin-specific localization. *Science Advances* **8**, eabk0793, doi:doi:10.1126/sciadv.abk0793 (2022).
80 Karslake, J. D. *et al.* SMAUG: Analyzing single-molecule tracks with nonparametric Bayesian statistics. *Methods* **193**, 16-26, doi:10.1016/j.ymeth.2020.03.008 (2021).
81 Heckert, A., Dahal, L., Tjian, R. & Darzacq, X. Recovering mixtures of fast-diffusing states from short single-particle trajectories. *eLife* **11**, e70169, doi:10.7554/eLife.70169 (2022).
82 Zhang, L. & Elias, J. E. Relative Protein Quantification Using Tandem Mass Tag Mass Spectrometry. *Methods Mol Biol* **1550**, 185-198, doi:10.1007/978-1-4939-6747-6_14 (2017).
83 Wang, J. *et al.* Epe1 recruits BET family bromodomain protein Bdf2 to establish heterochromatin boundaries. *Genes & Development* **27**, 1886-1902, doi:10.1101/gad.221010.113 (2013).
84 Hirano, Y., Asakawa, H., Sakuno, T., Haraguchi, T. & Hiraoka, Y. Nuclear Envelope Proteins Modulating the Heterochromatin Formation and Functions in Fission Yeast. *Cells* **9**, 1908 (2020).
85 Zofall, M., Sandhu, R., Holla, S., Wheeler, D., Grewal, S.I.S. Histone deacetylation primes self-propagation of heterochromatin domains to promote epigenetic inheritance. *Nature Structural & Molecular Biology* **29**, 898–909, doi:https://doi.org/10.1038/s41594-022-00830-7 (2022).
86 Shan, C.-M. *et al.* The INO80 Complex Regulates Epigenetic Inheritance of Heterochromatin. *Cell Reports* **33**, 108561, doi:https://doi.org/10.1016/j.celrep.2020.108561 (2020).
87 Takahata, S. *et al.* Two secured FACT recruitment mechanisms are essential for heterochromatin maintenance. *Cell Reports* **36**, 109540, doi:https://doi.org/10.1016/j.celrep.2021.109540 (2021).
88 Aygun, O., Mehta, S. & Grewal, S. I. HDAC-mediated suppression of histone turnover promotes epigenetic stability of heterochromatin. *Nat Struct Mol Biol* **20**, 547-554, doi:10.1038/nsmb.2565 (2013).
89 Kang, J. *et al.* Mitotic centromeric targeting of HP1 and its binding to Sgo1 are dispensable for sister-chromatid cohesion in human cells. *Mol Biol Cell* **22**, 1181-1190, doi:10.1091/mbc.E11-01-0009 (2011).
90 Roche, B., Arcangioli, B. & Martienssen, R. A. RNA interference is essential for cellular quiescence. *Science* **354**, doi:10.1126/science.aah5651 (2016).
91 Jacobs, S. A. & Khorasanizadeh, S. Structure of HP1 chromodomain bound to a lysine 9-methylated histone H3 tail. *Science* **295**, 2080-2083, doi:10.1126/science.1069473 (2002).

92 Jacobs, S. A. *et al.* Specificity of the HP1 chromo domain for the methylated N-terminus of histone H3. *Embo j* **20**, 5232-5241, doi:10.1093/emboj/20.18.5232 (2001).
93 Baumgartner, L. *et al.* The Drosophila ZAD zinc finger protein Kipferl guides Rhino to piRNA clusters. *eLife* **11**, doi:10.7554/eLife.80067 (2022).
94 Baumgartner, L. *et al.* Evolutionary adaptation of the chromodomain of the HP1-protein Rhino allows the integration of chromatin and DNA sequence signals. *bioRxiv*, 2023.2009.2029.560096, doi:10.1101/2023.09.29.560096 (2023).
95 Torres-Garcia, S. *et al.* Epigenetic gene silencing by heterochromatin primes fungal resistance. *Nature* **585**, 453-458, doi:10.1038/s41586-020-2706-x (2020).
96 Yaseen, I. *et al.* Proteasome-dependent truncation of the negative heterochromatin regulator Epe1 mediates antifungal resistance. *Nat Struct Mol Biol* **29**, 745-758, doi:10.1038/s41594-022-00801-y (2022).
97 Bao, K. *et al.* The cAMP signaling pathway regulates Epe1 protein levels and heterochromatin assembly. *PLOS Genetics* **18**, e1010049, doi:10.1371/journal.pgen.1010049 (2022).
98 Bao, K., Shan, C. M., Moresco, J., Yates, J., 3rd & Jia, S. Anti-silencing factor Epe1 associates with SAGA to regulate transcription within heterochromatin. *Genes Dev* **33**, 116-126, doi:10.1101/gad.318030.118 (2019).
99 Braun, S. *et al.* The Cul4-Ddb1(Cdt)² ubiquitin ligase inhibits invasion of a boundary-associated antisilencing factor into heterochromatin. *Cell* **144**, 41-54, doi:10.1016/j.cell.2010.11.051 (2011).
100 Bähler, J. *et al.* Heterologous modules for efficient and versatile PCR-based gene targeting in Schizosaccharomyces pombe. *Yeast* **14**, 943-951, doi:10.1002/(sici)1097-0061(199807)14:10<943::Aid-yea292>3.0.Co;2-y (1998).
101 Khare, A. K., Singh, B. & Singh, J. A fast and inexpensive method for random spore analysis in Schizosaccharomyces pombe. *Yeast* **28**, 527-533, doi:https://doi.org/10.1002/yea.1855 (2011).
102 Torres-Garcia, S. *et al.* SpEDIT: A fast and efficient CRISPR/Cas9 method for fission yeast. *Wellcome Open Res* **5**, 274, doi:10.12688/wellcomeopenres.16405.1 (2020).
103 Kitzman, J. O., Starita, L. M., Lo, R. S., Fields, S. & Shendure, J. Massively parallel single-amino-acid mutagenesis. *Nat Methods* **12**, 203-206, 204 p following 206, doi:10.1038/nmeth.3223 (2015).
104 Li, H. & Durbin, R. Fast and accurate long-read alignment with Burrows–Wheeler transform. *Bioinformatics* **26**, 589-595, doi:10.1093/bioinformatics/btp698 (2010).
105 Bolger, A. M., Lohse, M. & Usadel, B. Trimmomatic: a flexible trimmer for Illumina sequence data. *Bioinformatics* **30**, 2114-2120, doi:10.1093/bioinformatics/btu170 (2014).
106 Fineberg, A., Surrey, T. & Kukura, P. Quantifying the Monomer-Dimer Equilibrium of Tubulin with Mass Photometry. *J Mol Biol* **432**, 6168-6172, doi:10.1016/j.jmb.2020.10.013 (2020).
107 Cianfrocco, M. A., Wong-Barnum, M., Youn, C., Wagner, R. & Leschziner, A. in *Proceedings of the Practice and Experience in Advanced Research Computing 2017 on Sustainability, Success and Impact* 1-5 (2017).
108 Pettersen, E. F. *et al.* UCSF Chimera--a visualization system for exploratory research and analysis. *J Comput Chem* **25**, 1605-1612, doi:10.1002/jcc.20084 (2004).
109 Lim, Y. *et al.* In silico protein interaction screening uncovers DONSON's role in replication initiation. *Science* **381**, eadi3448, doi:doi:10.1126/science.adi3448 (2023).
110 Isaacoff, B. P., Li, Y., Lee, S. A. & Biteen, J. S. SMALL-LABS: Measuring Single-Molecule Intensity and Position in Obscuring Backgrounds. *Biophysical Journal* **116**, 975-982, doi:https://doi.org/10.1016/j.bpj.2019.02.006 (2019).
111 Munkres, J. Algorithms for the Assignment and Transportation Problems. *Journal of the Society for Industrial and Applied Mathematics* **5**, 32-38, doi:10.1137/0105003 (1957).

112 Rowland, D. J. & Biteen, J. S. Measuring molecular motions inside single cells with improved analysis of single-particle trajectories. *Chemical Physics Letters* **674**, 173-178 (2017).
113 Deutsch, E. W. *et al.* The ProteomeXchange consortium at 10 years: 2023 update. *Nucleic Acids Res* **51**, D1539-d1548, doi:10.1093/nar/gkac1040 (2023).
114 Perez-Riverol, Y. *et al.* The PRIDE database resources in 2022: a hub for mass spectrometry-based proteomics evidences. *Nucleic Acids Res* **50**, D543-d552, doi:10.1093/nar/gkab1038 (2022).